Wear 309 (2014) 174–191

Contents lists available at ScienceDirect

Wear

journal homepage: www.elsevier.com/locate/wear

Development of a wear model for the analysis of complex railway networks

A. Innocenti, L. Marini, E. Meli *, G. Pallini, A. Rindi

Department of Industrial Engineering, University of Florence, Via S. Marta n. 3, 50139 Firenze, Italy

ARTICLE INFO

Article history:
Received 24 July 2013
Received in revised form
6 November 2013
Accepted 9 November 2013
Available online 20 November 2013

Keywords:
Wheel–rail wear
Multibody modeling of railway vehicles
Statistical track analysis

ABSTRACT

In railway applications, the estimation of wear at the wheel–rail interface is an important field of study, mainly correlated to the planning of maintenance interventions, vehicle stability and the possibility of carrying out specific strategies for the wheel profile optimization. In this work the authors present a model for the evaluation of wheel and rail profile evolution due to wear specifically developed for complex railway networks. The model layout is made up of two mutually interactive but separate units: a vehicle model (composed of the multibody model and the global contact model) for the dynamical analysis and a model for the wear evaluation (composed of the local contact model, the wear evaluation procedure and the profile update strategy).

The authors propose a statistical approach for the railway track description to study complex railway lines in order to achieve general significant accuracy results in a reasonable time: in fact the exhaustive simulation of the vehicle dynamics and of wear evolution on all the railway network turn out to be too expensive in terms of computational effort for each practical purpose.

The wear model has been validated in collaboration with Trenitalia S.P.A and RFI, which have provided the technical documentation and the experimental data relating to some tests performed on a scenario that exhibits serious problems in terms of wear: the vehicle ALn 501 “Minuetto” circulating on the Aosta-Pre Saint Didier Italian line.

1. Introduction

The prediction of the wear phenomena at the wheel–rail interface is a fundamental issue in the railway field; in fact the consequent evolution of rail and wheel profiles involves serious effects on both dynamical and stability characteristics of vehicles. From a safety viewpoint, modifications in wheel and rail profiles may compromise the vehicle stability and also increase the derailment risk due to wheels climbing over the rail. Profile changes lead also to higher maintenance cost, mainly related to the periodical re-profiling operations of wheels and the undesirable replacements of rails, necessary to re-establish the original profiles. A reliable wear model can be used to optimize the original profiles of wheel and rail and to obtain a more uniform wear on the rolling surfaces. In such a way the overall amount of worn material can be reduced, the mean time between two maintenance interventions can be increased and, at the same time, the dynamical performance of the wheel–rail pair can be kept approximately constant between two succeeding repair interventions.

In this work the authors present a procedure to estimate the evolution of the wheel and rail profiles due to wear specifically developed for complex railway networks. The general layout of the model consists of two mutually interactive parts: the vehicle model (multibody model and 3D global contact model) and the wear model (local contact model, wear evaluation and profiles update) (see Fig. 1).

In the literature many important research works regarding wear models based both on global and local approaches to wear estimation can be found. Nowadays, both global and local approaches can be chosen to perform simulations by means of commercial multi-body softwares. In the global approach, often used by commercial multi-body software to reduce the computational load despite the model accuracy [1–3], the wear evolution is computed without taking into account the contact patch but hypothesizing that the contact between the surfaces occurs in a single point; in this way both underestimation and overestimation of the worn material are often possible. The local approaches [4–7], instead, subdivide the contact patch into adhesion and slip area, leading to more accurate results but increasing the computational time; some works in which the differences between global and local wear approaches are carefully investigated can be found in the literature [8].

However a substantial lack is present in the literature concerning wear models (both global and even more local) specifically

* Corresponding author. Tel.: +39 0554796286.
E-mail addresses: alice.innocenti@unifi.it (A. Innocenti), lorenzo.marini@unifi.it (L. Marini), enrico.meli@unifi.it, meli@mapp1.de.unifi.it (E. Meli), giovanni.pallini@unifi.it (G. Pallini), andrea.rindi@unifi.it (A. Rindi).

0043-1648/$ - see front matter © 2013 Elsevier B.V. All rights reserved.
http://dx.doi.org/10.1016/j.wear.2013.11.010

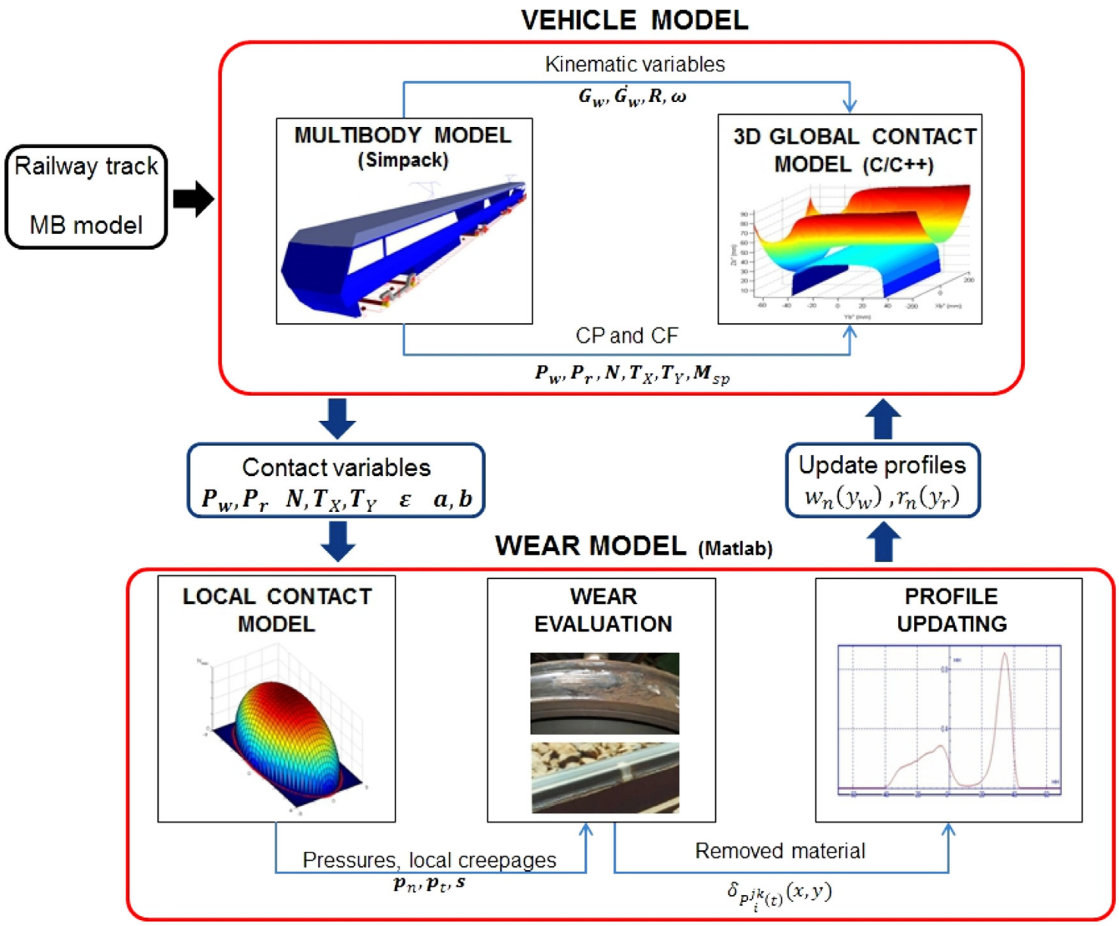

Fig. 1. General architecture of the model.

developed for complex railway network applications. In this case the computational load needed to carry out the exhaustive simulation of vehicle dynamics and wear evaluation turns out to be absolutely too high for each practical purpose. The authors previously worked on this issue [9], developing a wear model for the evaluation of wheel wear based on the local approach and statistical methods to reduce the computational time.

To overcome the main critical issue of wear prediction models, the authors propose a track statistical [1,10] approach to obtain relevant results in a reasonable time; more specifically the authors suggest the replacement of the entire railway net with a discrete set of N_c different curved tracks (classified by radius, superelevation and traveling speed) statistically equivalent to the original net. This approach allows a substantial reduction of the computational load and, at the same time, assures a good compromise in terms of model accuracy. In the literature, important results concerning this topic have been obtained in [10].

The present work has been carried out in collaboration with Trenitalia S.p.A. and RFI that provided the experimental data concerning the Aosta-Pre Saint Didier railway line and the vehicle ALSTOM *DMU Aln 501 Minuetto* (which in this scenario exhibits serious problems in terms of wear) necessary for the preliminary model validation.

2. General architecture of the model

The general architecture of the model developed for studying the wear phenomena on complex railway lines is shown in the block diagram in Fig. 1 in which two different main parts are present: the *vehicle model* necessary to perform the dynamical analysis and the *wear model*.

The *vehicle model* consists of the multibody model of the benchmark railway vehicle and the 3D global contact model that, during the dynamical simulation, interact directly online creating a loop. At each time integration step the first one evaluates the kinematic variables (position, orientation and their derivatives) relative to the wheelsets and consequently to each wheel–rail contact pair. At this point, starting from the kinematic quantities the 3D global contact model calculates the global contact variables (contact points and contact forces, contact areas and global creepages), this model is based both on an innovative algorithm for the detection of the contact points (developed by the authors in the previous works [11,12,26–29]) and on Hertz's and Kalker's global theories for the evaluation of the contact forces [13–15,21,25]. The global contact variables are then passed to the multibody model to carry on the vehicle dynamics simulation.

The dynamic simulations have been performed in the commercial Multibody Software (MBS) Simpack. In particular, the multibody model has been defined in the Simpack Rail environment, while the wheel–rail 3D global contact model, implemented in C/C++ language, has been customized by the authors through a specifically developed FORTRAN routine defined within the Simpack User routine module.

The main inputs of the *vehicle model* are the multibody model of the railway vehicle and the corresponding railway track, represented in this work by the ALSTOM *DMU Aln 501 Minuetto* and the Aosta-Pre Saint Didier line respectively (a critical scenario in Italian Railways in terms of both wear and stability). In wear estimation research activities the track description is a critical task

due to the complexity of the railway nets to be studied: in fact the exhaustive simulation of vehicle dynamics and of wear evolution on all the railway net turns out to be too expensive both concerning computation times and memory consumption and concerning the availability and the collection of the experimental data needed for the model validation. To overcome these limitations, a statistical approach [1,10] has been developed to achieve general significant results in a reasonable time; in particular the entire considered railway net has been replaced with a discrete set of N_c different curved tracks (classified by radius, superelevation and traveling speed) statistically equivalent to the original net. In this work both the track configurations (the whole Aosta Pre-Saint Didier line and the equivalent representation derived by means of statistical methods) will be described, focusing on the wear modeling differences between the two cases and comparing the obtained results from the efficiency and accuracy viewpoint.

The *wear model* is the part of the procedure concerning the prediction of the amount of worn material to be removed from the wheel and rail surfaces and is made up of three distinct phases: the local contact model [1], the wear evaluation and the profile update. The local contact model (based both on Hertz's local theory and on simplified Kalker's algorithm FASTSIM [14,16]), starting from the global contact variables, estimates the local contact pressures and creepages inside the contact patch and detects the slip zone of the contact area. Subsequently the distribution of removed material is calculated both on the wheel and on the rail surface only within the slip area by using an experimental relationship between the removal material and the energy dissipated by friction at the contact interface [17,18]. Finally wheel and rail worn profiles are derived from the original ones through an appropriate update strategy. The new updated wheel and rail profiles (one mean profile both for all the wheels of the vehicle and for all the considered tracks) are then fed back as inputs to the *vehicle model* and the whole model architecture can proceed with the next discrete step.

In particular, since the wear model is conceived to describe complex railway nets (composed by several different tracks traveled by different vehicles), it is natural to consider, at this step, the wear evolution of a mean profile both for wheel and rail without distinguishing the single wheels and the single tracks. However, the procedure for wear evaluation can be easily extended to simulate independent wear evolution of all wheels of the vehicle and of all rail profiles in each curve class. In such a way, also different initial conditions can be assigned to the profiles. The wear model has been fully implemented in the Matlab environment.

The evolution of wheel and rail profiles is consequently a discrete process. The choice of the discrete step should ensure a good balance between the model precision and the computational load and, as it will be clarified in the following, has to consider the difference between the time scales characterizing wheel and rail wear evolution rates. For the wheel wear prediction the total mileage km_{tot} traveled by the vehicle is subdivided into discrete steps with a suitable strategy and within each step (corresponding to km_{step} traveled by the vehicle) the wheel profile is supposed to be constant. For the rail, instead, the depth of the wear does not depend on the traveled distance but on the total tonnage M_{tot} burden on the track and thus on the number of vehicles moving on the track; in particular the total vehicle number N_{tot} will be subdivided into discrete steps (corresponding to N_{step} vehicle on the track) wherein the rail profile is supposed to be constant.

Among the several types of profile update procedures, the adaptive strategy has been chosen in this research activity [5,6]: it is based on the definition of a threshold value that imposes the maximum material quantity to be removed at each profile update, leading to a variable update step. If compared to a constant step update strategy, the adaptive step is more suitable to represent both the nonlinear behavior of wear evolution and the higher rate characterizing the first phases of wear evolution (both on wheel and rail) due to the initial non-conformal contact between the unworn profiles.

Both experimental data and dynamical simulations have been obtained, according to Trenitalia, on straight and curved tracks characterized by the same initial condition: UIC60 unworn rail profile canted at 1/20 rad and track gauge value equal to 1435 mm (all the tracks in Italian railway lines are characterized by the previous rail profile and track gauge value). When track data on Aosta-Pre Saint Didier line have been acquired, rails have been just re-profiled and thus were in the above-mentioned initial condition.

3. The vehicle model

In this section a brief description of the *vehicle model* is given. First of all the multibody model of the studied benchmark vehicle is introduced; then the 3D global contact model is explained.

3.1. The multibody model

The benchmark vehicle investigated for this research is the *DMU Aln 501 Minuetto*, a passenger transport unit widespread in Italian Railways, where it is equipped with the standard ORE S1002 wheel profile and UIC60 rail profile canted at 1/20 rad. This particular vehicle exhibits in fact severe wear and stability problems mainly caused by the adopted matching. Its mechanical structure and inertial, elastic and damping properties can be found in the literature [19,20].

In Table 1 the inertia properties of the vehicle are shown: motors and gear boxes have not been modeled and their inertia

Table 1
Inertia properties of the multibody model.

MBS body	Mass (kg)	Roll inertia (kg m^2)	Pitch inertia (kg m^2)	Yaw inertia (kg m^2)
Coach M	31,568	66,700	764,000	743,000
Coach T	14,496	30,600	245,000	236,000
Bogie m	3306	1578	2772	4200
Bogie t	3122	1674	3453	5011
Wheelset m	2091	1073	120	1073
Wheelset t	1462	1027	120	1027

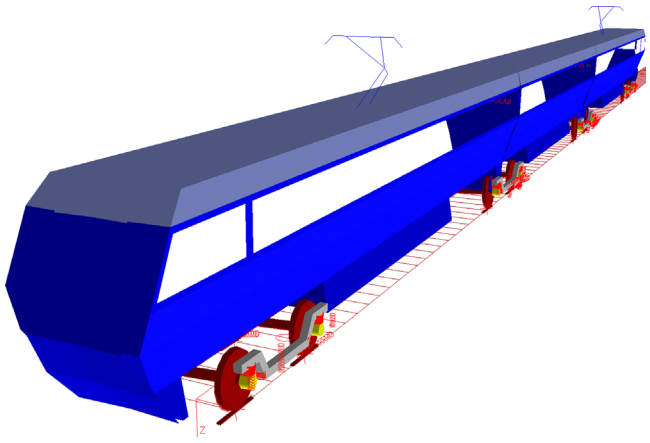

Fig. 2. Global view of the multibody model.

properties have been included in the motor bogie and in the motor wheelset (indicated in Table 1 with **Bogie m** and **Wheelset m** respectively) to take into account their different influence on the unsprung and sprung mass. The multibody model has been realized in the Simpack Rail environment (see Fig. 2) and consists of 31 rigid bodies:

- three coaches;
- four bogies: the intermediate ones, interposed between two successive coaches, are trailer bogies while the other ones are motor bogies;
- eight wheelsets: two for each bogie;
- 16 axleboxes: two for each wheelset.

The rigid bodies are connected by means of appropriate elastic and damping elements; more specifically the vehicle is equipped with two suspension stages. The primary suspensions connect the wheelsets to the bogies (see Fig. 3) and comprise two springs and two vertical dampers, while the secondary suspensions connect the bogies to the coaches (see Fig. 4) and comprise two air springs, six non-linear dampers (lateral, vertical and anti-yaw dampers), one non-linear traction rod, the roll bar (not visible in the figure) and two non-linear lateral bumpstops.

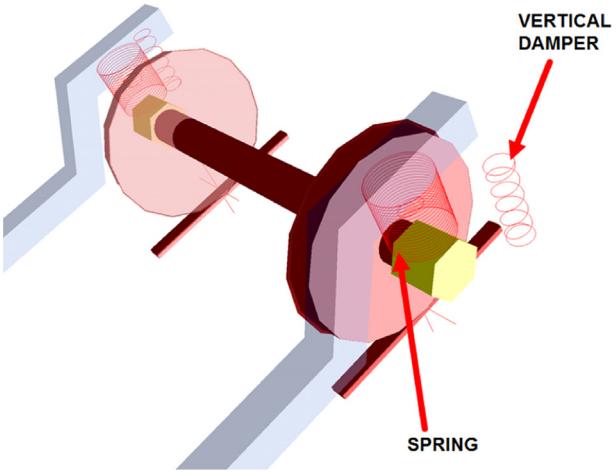

Fig. 3. Primary suspensions.

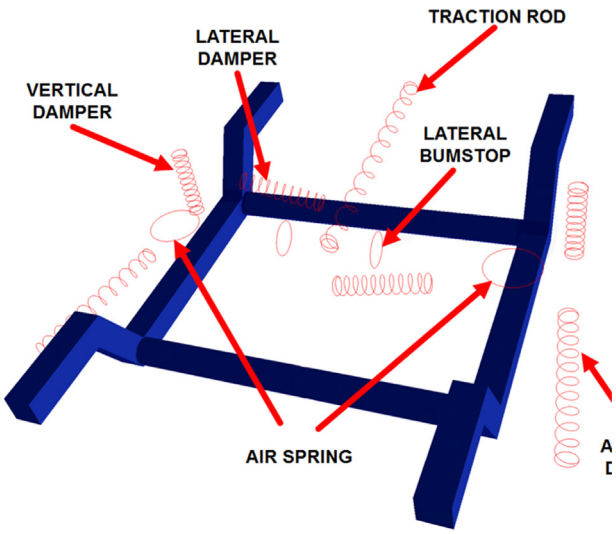

Fig. 4. Secondary suspensions.

Table 2
Main linear stiffness properties of the ALn 501 "Minuetto".

Primary suspension	
Flexicoil k_z	9.01×10^5 N/m
Flexicoil k_x, k_y	1.26×10^6 N/m
Sutuco bushing k_x	2.0×10^7 N/m
Sutuco bushing k_y	1.5×10^7 N/m
Secondary suspension	
Airspring k_z	3.98×10^5 N/m
Airspring k_x, k_y	1.2×10^5 N/m
Anti-roll bar k_α	2.6×10^6 Nm/rad
Coach connection	
Bushing k_x, k_z	7.24×10^7 N/m
Bushing k_y	5.2×10^6 N/m

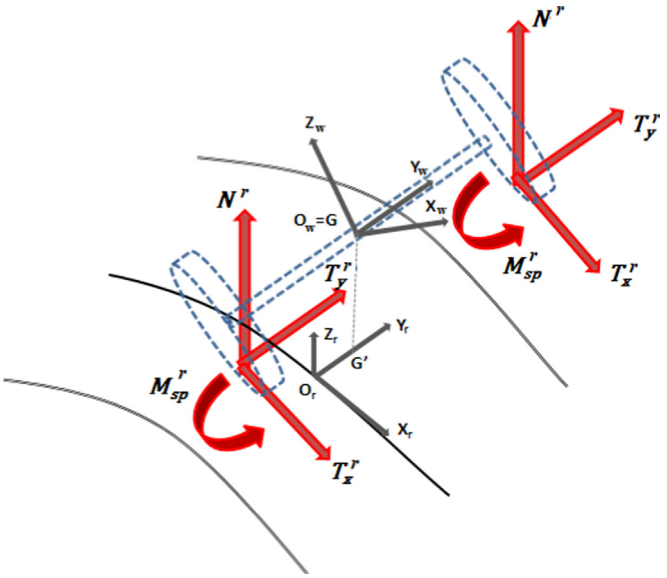

Fig. 5. Global forces acting at wheel and rail interface.

Both the stages of suspensions have been modeled by means of three-dimensional viscoelastic force elements taking into account all the mechanical non-linearities of the system (bumpstop clearance, dampers and rod behavior). The main linear characteristics of the suspensions are shown in Table 2 while the nonlinear characteristics are imposed as a function of displacement and velocity for springs and dampers.

3.2. The global contact model

In the present work a specifically developed 3D global contact model has been adopted to improve reliability and accuracy of the contact points detection. The main features of the innovative adopted algorithm, when compared with the current state of the art of the contact models employed in railway field [1,21,25], are the following [22,12,11,26–29]:

- it is a fully 3D model that takes into account all the six relative degrees of freedom (DOF) between wheel and rail;
- it is able to support generic railway tracks and generic wheel and rail profiles;
- it does not introduce any limits on the number of detected contact points;
- it assures a general and accurate treatment of the multiple contact without introducing simplifying assumptions on the problem geometry and kinematics, such as the partition of wheel and rail profiles in zones, which is adopted to get an

easier localization of the contact points and used in many commercial software [1];
- it assures highly numerical efficiency making possible the online implementation within the commercial multibody software (Simpack-Rail, Adams-Rail) without look-up table; in this way also the numerical performances of the commercial multibody software are improved.

As shown in Fig. 1, the global contact model inputs are the kinematic variables evaluated by the multibody model, i.e. the position, the orientation matrix R_w^r, the absolute velocity $\dot{\mathbf{O}}_w^r$ and the absolute angular velocity $\boldsymbol{\omega}_w^r$ of the wheelset (where the apexes w and r refer respectively to the wheel $O_w x_w y_w z_w$ and rail $O_r x_r y_r z_r$ reference systems shown in Fig. 5).

Starting from these inputs, the global contact model previously developed by the authors evaluates the following outputs: positions $\mathbf{P}_w^r$ and $\mathbf{P}_r^r$ of the contact points on wheel and rail respectively, the normal $\mathbf{N^r}$ and tangential $\mathbf{T_x^r}$ and $\mathbf{T_y^r}$ contact forces and the spin moment $\mathbf{M_{sp}^r}$, the global creepages $\boldsymbol{\varepsilon}$. Always referring to the reference systems $O_r x_r y_r z_r$ and $O_w x_w y_w z_w$ (Fig. 5), wheel and rail profiles are denoted respectively as $w(y_w)$ and $r(y_r)$.

In particular the adopted contact model is based on a two step procedure; at the first step the contact points number and positions are determined through an innovative algorithm designed and validated by the authors [22,12,11]. During the second step, for each detected contact point, the global contact forces (Fig. 5) are computed using Hertz's and Kalker's global theories [15,13]. These theories have been chosen because they represent a good compromise between accuracy and efficiency.

The contact point detection algorithm developed by the authors is based on the analytical reduction of the algebraic contact problem dimension (from a 4D problem to a simply 1D scalar problem) by means of exact analytical procedures that leads to an increase in accuracy and numerical efficiency of the contact model. More specifically the new wheel–rail contact point detection procedure employed in the present research activity is called *distance method*; it starts from the multi-dimensional formulation of the contact problem and reduces it to a simple mono-dimensional scalar problem. The distance method is derived starting from the two following vectorial equations (which represent a common formulation of the contact problem in multibody applications):

$$\mathbf{n}_r^r(\mathbf{P}_r^r) \wedge \mathbf{n}_w^r(\mathbf{P}_w^r) = \mathbf{n}_r^r(\mathbf{P}_r^r) \wedge R_w^r \mathbf{n}_w^w(\mathbf{P}_w^w) = \mathbf{0} \tag{1a}$$

$$\mathbf{n}_r^r(\mathbf{P}_r^r) \wedge \mathbf{d}^r = \mathbf{0} \tag{1b}$$

representing respectively the parallelism condition between the outgoing normal unit vector $\mathbf{n}_w^w(\mathbf{P}_w^w)$ to the wheel surface and the outgoing normal unit vector to the rail surface $\mathbf{n}_r^r(\mathbf{P}_r^r)$ and the parallelism between the outgoing unit vector of the rail surface and the distance vector $\mathbf{d}^r = \mathbf{P}_r^r - \mathbf{P}_r^w$, which indicates the distance between two generic points on the wheel surface and on the rail surface.

The system (1) results in six nonlinear equations in the four unknowns, but only four of these equations are independent; hence the real problem dimension is 4D. By means of an exact analytical procedure it is possible to express three of these variables as a function of the remaining one, with a consequent reduction of the original 4D problem to a simple 1D scalar equation.

4. The wear model

In this section the three phases in which the wear model has been divided will be described in detail.

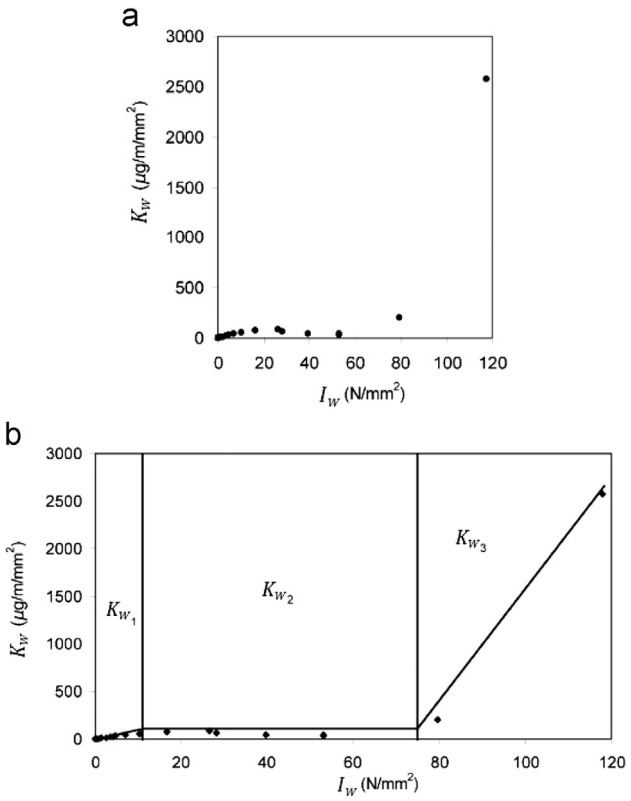

Fig. 6. Trend of the *wear rate* K_W [4,8,17]. (a) Experimental data. (b) Wear regimes.

4.1. The local contact model

The inputs of the wear model are the global contact parameters estimated by the vehicle model. Since a local wear computation is required [1], the global contact parameters need to be post-processed and this can be achieved through the simplified Kalker's theory implemented in the FASTSIM algorithm which represents a good compromise between accuracy and efficiency. This theory starts from global creepages (ε_x, ε_y, ε_{sp}), normal and tangential global forces (N^r, T_x^r, T_y^r), contact patch dimensions (a, b) and material properties to compute the local distribution of normal p_n and tangential $\mathbf{p}_t$ stresses and local slip $\mathbf{s}$ across the wheel–rail contact area. For a more detailed description of the FASTSIM algorithm one can refer to the literature [16].

4.2. The wear evaluation

To evaluate the specific volume of removed material on wheel and rail due to wear $\delta_{P_{wi}^j(t)}(x,y)$ and $\delta_{P_{ri}^j(t)}(x,y)$ (where x and y indicate respectively the coordinates of a generic point of the contact patch related to the i-th contact points $P_{wi}^j(t)$ and $P_{ri}^j(t)$ on the j-th wheel and rail pair for unit of distance traveled by the vehicle, expressed in m, and for unit of surface, expressed in mm), an experimental relationship between the volume of removed material and the frictional work [17,18] has been used. More specifically, local contact stresses $\mathbf{p}_t$ and slip $\mathbf{s}$ are used to evaluate the *wear index* I_W (expressed in N/mm^2), which represents the frictional power generated by the tangential contact pressures $I_W = \mathbf{p}_t \cdot \mathbf{s}/V$ where V is the longitudinal speed.

This index can be correlated with the *wear rate* K_W that is the mass of removed material (expressed in $\mu g/m\,mm^2$) for unit of distance traveled by the vehicle and for unit of surface. The correlation is based on real data available in the literature [4,8,17,7], which have been acquired from experimental wear tests

carried out in the case of metal to metal contact using a twin disc test arrangement. The test discs are hydraulically loaded together and driven at controlled rotational speed by independent electric motors; shaft encoders monitor the speeds continuously. A torque transducer is assembled on one of the drive shafts and a load cell is mounted beneath the hydraulic jack. The slip ratio required is achieved by adjustment of the rotational speeds. These tests were carried out under dry condition without lubrication (resulting in a frictional coefficient of 0.45–0.50) considering the coupling between discs made of R8T steel for the wheel and UIC60 900A steel for the rail [4,8,17] and measuring the mass loss during the tests; the considered couple of material is widely used in European and Italian railways and also for the vehicle and the tracks analyzed in this research. The experimental relationship between K_W and I_W adopted for the current wear model is shown in Fig. 6.

In order to provide wear coefficients for use in the wheel wear modeling procedure the wear rate data was split into three regions (see Fig. 6(b)). A wear coefficient was defined for each of these regions [4,8,17]:

$$K_W(I_W) = \begin{cases} 5.3 * I_W & I_W < 10.4 \\ 55.1 & 10.4 \le I_W \le 77.2 \\ 61.9 * I_W - 4778.7 & I_W > 77.2. \end{cases} \quad (2)$$

Because of the lack of experimental data generated in the third regime, there may be the possibility of less accurate wear predictions for contacts at these conditions. However the wheel–rail contact is in K_{W1} and K_{W2} regions mostly if not all of the time and only reaches K_{W3} region in the most severe curves.

From a physical viewpoint [4,8,17], at low I_W oxidative wear was seen to occur on both wheel and rail discs. At the surfaces the oxide layer is just visible and there is a very small amount of deformation just below the wear surface of the discs. As I_W was increased, the wear mechanism altered and the wheel material appeared to wearing by a delamination process. A larger amount of plastic deformation was occurring below the wheel disc wear surface and crack formation just below the surface was visible leading to thin slivers of material breaking away from the surface. Finally as I_W was increased further these cracks were seen to alter direction from running parallel to the wear surface and turning up to turning down into the material causing larger chunks of material to break away. The wear features and mechanisms are discussed in greater detail in [4,8,17].

Since in this research activity a local wear model is developed, the wear law (2) is used in a local version, relating directly the tangential contact pressures (see the expression of I_W) with the amount of removed material due to wear (see the definition of K_W).

Once the wear rate $K_W(I_W)$ is known (the same both for the wheel and for the rail), the specific volume of removed material on the wheel and on the rail (for unit of distance traveled by the vehicle and for unit of surface) can be calculated as follows (expressed in $mm^3/m\,mm^2$):

$$\delta_{P^j_{wi}(t)}(x,y) = K_W(I_W)\frac{1}{\rho} \quad \delta_{P^j_{ri}(t)}(x,y) = K_W(I_W)\frac{1}{\rho} \quad (3)$$

where ρ is the material density (expressed in kg/m).

It must be noticed that, at the present state of the research activity, all the results have been obtained adopting the wear parameters specified in the literature [4,8,17] without any wear model tuning.

4.3. The profile update procedure

After obtaining the amount of worn material, wheel and rail profiles need to be updated to be used as the input of the next step of the whole model. The new profiles, denoted by $w_n(y_w)$ and $r_n(y_r)$, are computed from the old ones $w_o(y_w)$, $r_o(y_r)$ and from all

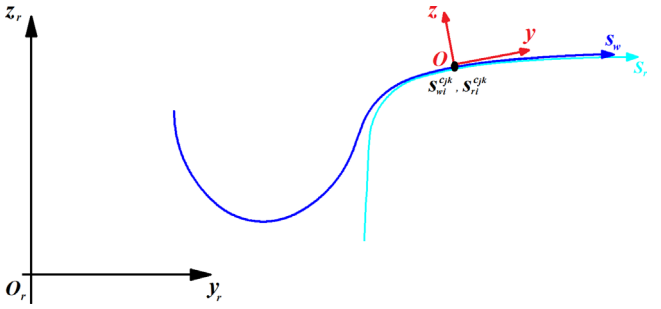

Fig. 7. Normal abscissa for the wheel and rail profiles.

the calculated distributions $\delta_{P^j_{wi}(t)}(x,y)$ and $\delta_{P^j_{ri}(t)}(x,y)$ of worn material through an appropriate set of numerical procedures that defines the update strategy:

- *Longitudinal integration*:

$$\frac{1}{2\pi w(y^j_{wi})}\int_{--a(y)}^{+a(y)} \delta_{P^j_{wi}(t)}(x,y)\,dx = \delta^{tot}_{P^j_{wi}(t)}(y) \quad (4)$$

$$\frac{1}{l_{sim}}\int_{--a(y)}^{+a(y)} \delta_{P^j_{ri}(t)}(x,y)\,dx = \delta^{tot}_{P^j_{ri}(t)}(y) \quad (5)$$

where $a(y)$ is the longitudinal length of the contact patch (evaluated in y), $w(y^j_{wi})$ is the wheel radius evaluated in $y_{wi}{}^j$ and l_{sim} is the length of the simulated track (when the complete railway track of length l_{track} is simulated $l_{sim} = l_{track}$, while in the statistical analysis case $l_{sim} = l_{ct}$ with l_{ct} equal to the length of each of the N_c curved tracks). This preliminary integration provides the mean value of removed material (expressed in $mm^3/(m\,mm^2)$) in the longitudinal direction. The difference between the terms $1/l_{sim}$ and $1/2\pi w(y^j_{wi})$ (with the track length much greater than the wheel circumference length) is the main cause that leads the wheel to wear much faster than the rail and consequently to a different scale of magnitude of the two investigated phenomena. This reflects the real physical behavior where the life of the rail is much greater than that of the wheel.

- *Track integration*:

$$\int_{T_{in}}^{T_{end}} \delta^{tot}_{P^j_{wi}(t)}(y)V(t)dt \approx \int_{T_{in}}^{T_{end}} \delta^{tot}_{P^j_{wi}(t)}(s_w - - s^{cj}_{wi}(t))V(t)dt = \Delta_{P^j_{wi}}(s_w) \quad (6)$$

$$\int_{T_{in}}^{T_{end}} \delta^{tot}_{P^j_{ri}(t)}(y)V(t)dt \approx \int_{T_{in}}^{T_{end}} \delta^{tot}_{P^j_{ri}(t)}(s_r - - s^{cj}_{ri}(t))V(t)dt = \Delta_{P^j_{ri}}(s_r); \quad (7)$$

the track integration sums all the wear contributes of the dynamic simulations to obtain the depth of removed material for wheel $\Delta_{P^j_{wi}}(s_w)$ and rail $\Delta_{P^j_{ri}}(s_r)$ expressed in $mm = mm^3/mm^2$. The introduction of the natural abscissas s_w and s_r of the curves $w(y_w)$ and $r(y_r)$ respectively leads to a better accuracy in the calculation of the worn profiles. In particular the following expressions locally hold (see Fig. 7):

$$y \approx s_w - s^{cj}_{wi}(t) \quad y \approx s_r - s^{cj}_{ri}(t) \quad (8)$$

$$w(y_w) = w(y_w(s_w)) = \tilde{w}(s_w) \quad r(y_r) = r(y_r(s_r)) = \tilde{r}(s_r) \quad (9)$$

where the natural abscissas of the contact points s^{cj}_{wi} and s^{cj}_{ri} can be evaluated from their positions P^j_{wi} and P^j_{ri} respectively.

- *Sum on the contact points*:

$$\sum_{i=1}^{N_{PDC}} \Delta_{P^j_{wi}}(s_w) = \Delta^w_j(s_w) \quad \sum_{i=1}^{N_{PDC}} \Delta_{P^j_{ri}}(s_r) = \Delta^r_j(s_r) \quad (10)$$

where N_{PDC} is the maximum number of contact points of each

single wheel (and respectively of each single rail); the amount of worn material related to non-active contact points (the number of active contact points changes during the simulation) is automatically set equal to zero.

- *Average on the wheel–rail pairs*:

$$\frac{1}{N_w}\sum_{j=1}^{N_w}\Delta_j^w(s_w)=\overline{\Delta}^w(s_w)\quad \frac{1}{N_w}\sum_{j=1}^{N_w}\Delta_j^r(s_r)=\overline{\Delta}^r(s_r) \tag{11}$$

where N_w is the number of vehicle wheels. The average on the number of wheel–rail pairs has to be evaluated in order to obtain as output of the wear model a single average profile both for the wheel and for the rail.

- *Average on the curved tracks of the statistical approach*: This step of the update procedure is important when a statistical description of the track is adopted. In this case different wear distributions $\overline{\Delta}_k^w(s_w)$ and $\overline{\Delta}_k^r(s_r)$ for each of the N_c curve classes will be obtained from the previous steps (with $1\le k\le N_c$). At this point the statistical weights p_k of the curve classes, calculated as the ratio between the track length characterized by the curve conditions related to the k-th class (in terms of radius and superelevation values) and the total railway track length, have to be introduced to consider the frequency with which each curve appears on the actual railway track. Consequently for the statistical approach the following relationships hold:

$$\sum_{k=1}^{N_c}p_k\overline{\Delta}_k^w(s_w)=\overline{\Delta}_{stat}^w(s_w)\quad \sum_{k=1}^{N_c}p_k\overline{\Delta}_k^r(s_r)=\overline{\Delta}_{stat}^r(s_r) \tag{12}$$

with $\sum_{k=1}^{N_c}p_k=1$ (see also Section 5.2). Obviously, when the dynamic simulations are performed on the complete railway track Eq. (12) simply becomes

$$\overline{\Delta}^w(s_w)=\overline{\Delta}_{track}^w(s_w)\quad \overline{\Delta}^r(s_r)=\overline{\Delta}_{track}^r(s_r). \tag{13}$$

- *Scaling*: Since it normally takes traveled distance of thousands kilometers in order to obtain measurable wear effects, an appropriate scaling procedure is necessary to reduce the simulated track length with a consequent limitation of the computational effort. Hypothesizing the almost linearity of the wear model with the traveled distance inside the discrete steps (valid if the discretization step length km_{step} is small enough to consider negligible the profile variation between two consequent steps), it is possible to amplify the removed material during the dynamic simulations by means of a scaling factor which increases the distance traveled by the vehicle.
  The linearity hypothesis is equivalent to suppose that the wear rate inside the simulated distance (km_{prove}) remains the same also inside the discrete step km_{step} (reasonable since the considered vehicle repeats the same railway track both during the simulated distance (km_{prove}) and during the discrete step (km_{step})).
  In this work adaptive discrete steps (function of wear rate and obtained imposing the threshold values D_{step}^w and D_{step}^r on the maximum of the removed material quantity on the wheelsets and on the tracks at each discrete step) have been chosen to update the wheel and rail profiles (see Eq. (14) and Fig. 8). The evaluation of the discrete steps, with the consequent scaling of $\overline{\Delta}_{stat}^w(s_w)$, $\overline{\Delta}_{track}^w(s_w)$ and $\overline{\Delta}_{stat}^r(s_r)$, $\overline{\Delta}_{track}^r(s_r)$, represents the major difference between the update strategy of wheel and rail:

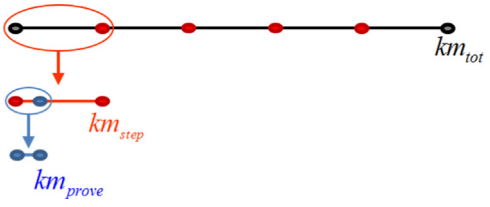

Fig. 8. Discretization of the total mileage.

1. The removed material on the wheel due to wear is proportional to the distance traveled by the vehicle; in fact a point of the wheel is frequently in contact with the rail in a number of times proportional to the distance. The following nomenclature can be introduced (see Fig. 8):
   - km_{tot} is the total mileage traveled by the considered vehicle and its value can be chosen depending on the purpose of the simulations [23];
   - km_{step} is the length of the discrete step corresponding to the threshold value on wear depth D_{step}^w;
   - km_{prove} is the overall mileage traveled by the vehicle during the dynamic simulations. This parameter assumes a different value according to the different way in which the track is treated: if the wear evolution is evaluated on the overall railway track (characterized by a length l_{track}) then $km_{prove}^{track}=l_{track}$ while, if the track statistical approach is considered, $km_{prove}^{stat}=l_{ct}$ is the mileage traveled by the vehicle during each of the N_c dynamic simulations. This consideration explains the deep difference in terms of computational load between the two considered cases; in the statistical analysis one, the necessity of acceptable computational time for the multibody simulations leads to the adoption of small values of the curve tracks length km_{prove}^{stat}, while in the total track one the km_{prove}^{track} value is imposed by the real track length with an inevitable increase in computational time.

   Finally the material removed on the wheels and the corresponding km_{step} value have to be scaled according to the following laws:

$$\overline{\Delta}_{stat}^w(s_w)\frac{D_{step}^w}{D_{stat}^w}=\overline{\Delta}_{stat}^{w\ sc}(s_w),\quad km_{step}^{stat}=\frac{D_{step}^w}{D_{stat}^w}km_{prove}^{stat} \tag{14}$$

$$\overline{\Delta}_{track}^w(s_w)\frac{D_{step}^w}{D_{track}^w}=\overline{\Delta}_{track}^{w\ sc}(s_w),\quad km_{step}^{track}=\frac{D_{step}^w}{D_{track}^w}km_{prove}^{track} \tag{15}$$

   where

$$D_{stat}^w=\max_{s_w}\overline{\Delta}_{stat}^w(s_w)\quad D_{track}^w=\max_{s_w}\overline{\Delta}_{track}^w(s_w). \tag{16}$$

   The choice of the spatial step km_{step} (and consequently of the threshold value D_{step}^w) must be a good compromise between numerical efficiency and the accuracy required by the wear model.
2. The depth of rail wear is not proportional to the distance traveled by the vehicle; in fact the rail tends to wear out only in the zone where it is crossed by the vehicle and, increasing the traveled distance, the depth of removed material remains the same. On the other side the rail wear is proportional to the total tonnage M_{tot} burden on the rail and thus to the total vehicle number N_{tot} moving on the track. Therefore, if N_{step} is the vehicle number moving in a discrete step, the quantity of rail removed material at each step will be

$$\overline{\Delta}_{stat}^r(s_r)\frac{D_{step}^r}{D_{stat}^r}=\overline{\Delta}_{stat}^r sc(s_r),\quad N_{step}^{stat}=\frac{D_{step}^r}{D_{stat}^r}N_{prove}^{stat} \tag{17}$$

$$\overline{\Delta}_{track}^r(s_r)\frac{D_{step}^r}{D_{track}^r}=\overline{\Delta}_{track}^r sc(s_r),\quad N_{step}^{track}=\frac{D_{step}^r}{D_{track}^r}N_{prove}^{track} \tag{18}$$

   where $N_{prove}^{stat}=N_c$, obviously $N_{prove}^{track}=1$ and

$$D^r_{stat} = \max_{s_r} \overline{\Delta}^r_{stat}(s_r) \quad D^r_{track} = \max_{s_r} \overline{\Delta}^r_{track}(s_r). \tag{19}$$

- *Smoothing of the removed material*:

$$\Im\left[\overline{\Delta}^{w\ sc}_{stat}(s_w)\right] = \overline{\Delta}^{w}_{stat_{sm}}{}^{sc}(s_w), \quad \Im\left[\overline{\Delta}^{w\ sc}_{track}(s_w)\right] = \overline{\Delta}^{w}_{track_{sm}}{}^{sc}(s_w) \tag{20}$$

$$\Im\left[\overline{\Delta}^{r\ sc}_{stat}(s_r)\right] = \overline{\Delta}^{r}_{stat_{sm}}{}^{sc}(s_r), \quad \Im\left[\overline{\Delta}^{r\ sc}_{track}(s_r)\right] = \overline{\Delta}^{r}_{track_{sm}}{}^{sc}(s_r); \tag{21}$$

the numerical noise and short spatial wavelengths without physical meaning that affect the worn material distributions can be passed to the new profiles $\tilde{w}^{stat}_n(s_w)$, $\tilde{w}^{track}_n(s_w)$ and $\tilde{r}^{stat}_n(s_r)$, $\tilde{r}^{track}_n(s_r)$ with consequent problems raising in the global contact model. Hence an appropriate smoothing of the worn material distributions is required. In this case it is achieved by means of a first-order discrete filter (i.e. a moving average filter with window size equal to 1%−5% of the total number of points in which the profiles are discretized); obviously the discrete filter has to conserve the mass.

- *Profile update:*

$$\begin{pmatrix} y_w(s_w) \\ \tilde{w}^{stat}_o(s_w) \end{pmatrix} - -\overline{\Delta}^{w}_{stat_{sm}}{}^{sc}(s_w)\mathbf{n}^r_w \overset{re-parameterization}{\longrightarrow} \begin{pmatrix} y_w(s_w) \\ \tilde{w}^{stat}_n(s_w) \end{pmatrix}$$

$$\begin{pmatrix} y_w(s_w) \\ \tilde{w}^{track}_o(s_w) \end{pmatrix} - -\overline{\Delta}^{w}_{track_{sm}}{}^{sc}(s_w)\mathbf{n}^r_w \overset{re-parameterization}{\longrightarrow} \begin{pmatrix} y_w(s_w) \\ \tilde{w}^{track}_n(s_w) \end{pmatrix}$$

$$\begin{pmatrix} y_r(s_r) \\ \tilde{r}^{stat}_o(s_r) \end{pmatrix} - -\overline{\Delta}^{r}_{stat_{sm}}{}^{sc}(s_r)\mathbf{n}^r_r \overset{re-parameterization}{\longrightarrow} \begin{pmatrix} y_r(s_r) \\ \tilde{r}^{stat}_n(s_r) \end{pmatrix}$$

$$\begin{pmatrix} y_r(s_r) \\ \tilde{r}^{track}_o(s_r) \end{pmatrix} - -\overline{\Delta}^{r}_{track_{sm}}{}^{sc}(s_r)\mathbf{n}^r_r \overset{re-parameterization}{\longrightarrow} \begin{pmatrix} y_r(s_r) \\ \tilde{r}^{track}_n(s_r) \end{pmatrix}; \tag{22}$$

the last step consists in the update of the old profiles $\tilde{w}^{stat}_o(s) = w^{stat}_o(y)$, $\tilde{w}^{track}_o(s) = w^{track}_o(y)$ and $\tilde{r}^{stat}_o(s_r) = r^{stat}_o(y_r)$, $\tilde{r}^{track}_o(s_r) = r^{track}_o(y_r)$ to obtain new profiles $\tilde{w}^{stat}_n(s) = w^{stat}_n(y)$, $\tilde{w}^{track}_n(s) = w^{track}_n(y)$ and $\tilde{r}^{stat}_n(s_r) = r^{stat}_n(y_r)$, $\tilde{r}^{track}_n(s_r) = r^{track}_n(y_r)$; since the removal of material occurs in the normal direction to the profiles ($\mathbf{n^r_w}$ and $\mathbf{n^r_r}$ are the outgoing unit vectors for the wheel and rail profiles respectively), once the quantities $\overline{\Delta}^{w}_{stat_{sm}}{}^{sc}(s_w)$, $\overline{\Delta}^{w}_{track_{sm}}{}^{sc}(s_w)$ and $\overline{\Delta}^{r}_{stat_{sm}}{}^{sc}(s_r)$, $\overline{\Delta}^{r}_{track_{sm}}sc(s_r)$ have been removed a re-parameterization of the profiles is needed in order to obtain again curves parameterized by means of the curvilinear abscissa.

5. Railway track description

In this section the two different strategies for the track description used in the present work will be presented.

5.1. The Aosta-Pre Saint Didier line

The whole Aosta-Pre Saint Didier railway network (characterized by an approximate length of $l_{track} \approx 31$ km) has been reconstructed and modeled in the Simpack environment starting from the track data provided by RFI. This is a very sharp track on the Italian Railways and the scenario is rather interesting since the *DMU Aln 501 Minuetto* exhibits serious problems on this track in terms of wear, requiring frequent maintenance interventions on the wheelsets.

In the next subparagraphs the experimental data provided by Trenitalia related to the wheel wear consisting in the wear control parameters measured as a function of the total distance traveled by the *DMU Aln 501 Minuetto* will be introduced.

5.1.1. Wear control parameters

The reference quotas FH, FT and QR are capable of estimating the wheel profile evolution due to wear without necessarily knowing the whole profile shape (see Fig. 9). In fact, the complete detection of the wheel profile is a long-lasting process that makes vehicle unavailable for the service for a long time. According to these parameters the user will be able both to establish when the worn wheel profile will have to be re-profiled and to detect if wear compromises dynamical stability of the vehicle [23].

As regards their physical meaning, both flange thickness FT and flange height FH describe the size of the flange: variations of the first quota are due to the action of wear which progressively reduces the thickness of flange and its structural resistance, while the rise of the flange height is a measure of wear on wheel tread. Otherwise, QR dimension is a shape parameter which quantifies the local conicity on the flange.

An additional control parameter is then introduced to evaluate the evolution of rail wear. Particularly the QM quota is defined as the rail head height in the point $y_r = 760$ mm with respect to the center line of the track: this y_r value depends on the railway gauge (equal to 1435 mm in the Aosta-Pre Saint Didier line) and on the laying angle α_p of the track (equal to 1/20 rad). Physically the QM quota gives information on the rail head wear (see Fig. 10).

5.1.2. Experimental data

The experimental data provided by Trenitalia have been measured on three different vehicles *DMU Aln 501 Minuetto* operating on the Aosta-Pre Saint Didier track that are conventionally called DM061, DM068, DM082. A mean value of the kinematic friction coefficient equal to $\mu_c = 0.28$ has been chosen (typical of the most frequent operating conditions).

As it can be seen by example in Table 3 for the vehicle MD061, the reference quota values have been measured for all the vehicle wheels (each vehicle has eight wheelsets and thus 16 wheels as specified in Section 3.1). To obtain as output a single average wheel profile that could be effectively compared with the profile extracted from the numerical simulation and to reduce the measurement errors, the arithmetic mean on all the 16 vehicle wheels has been evaluated and finally a scaling of the quota values has been carried out to delete the offset on the initial value of the considered quantities and impose the nominal values for all the

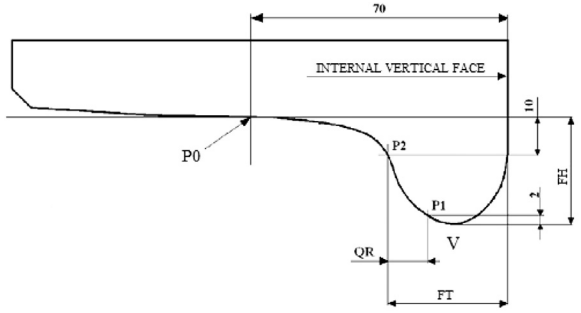

Fig. 9. Definition of the wheel wear control parameters.

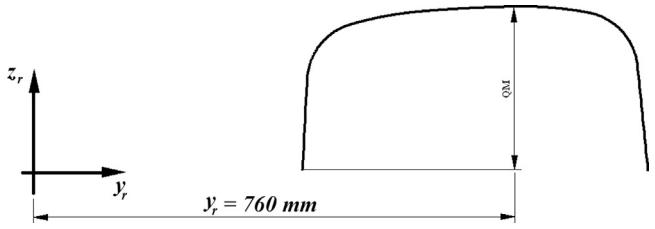

Fig. 10. Definition of rail wear control parameter.

Table 3
Experimental data of the *DMU Aln 501 Minuetto* DM061.

km	Quotas	1r	1l	2r	2l	3r	3l	4r	4l	5r	5l	6r	6l	7r	7l	8r	8l
		Wheel diameter 816 mm		Wheel diameter 815 mm		Wheel diameter 824 mm		Wheel diameter 823 mm		Wheel diameter 823 mm		Wheel diameter 823 mm		Wheel diameter 819 mm		Wheel diameter 820 mm	
0	FT	32.453	32.444	32.483	32.384	32.599	31.457	31.438	32.576	31.901	31.867	32.330	32.487	31.937	32.217	32.352	32.433
	FH	27.970	27.894	28.141	28.043	27.969	28.187	28.030	28.271	28.245	27.918	28.141	27.982	28.013	27.937	28.333	27.883
	QR	10.208	10.540	10.824	10.857	10.620	10.706	10.679	11.233	10.732	10.845	10.764	10.619	10.821	10.900	10.738	10.796
1426	FT	31.355	30.477	31.783	30.817	31.618	30.883	31.652	30.950	31.296	31.299	31.788	30.983	31.302	30.585	31.767	30.816
	FH	28.010	27.923	28.104	28.108	28.000	28.249	28.095	28.278	28.248	28.284	28.247	28.030	28.997	28.003	30.383	27.919
	QR	9.297	8.626	9.822	9.356	9.744	9.149	9.951	9.472	10.035	10.167	10.173	9.163	9.993	9.283	10.075	9.162
2001	FT	30.556	29.998	31.222	30.378	30.941	30.167	30.129	30.217	30.653	29.601	31.239	30.341	30.566	29.947	31.125	30.277
	FH	27.990	27.880	28.161	28.080	29.998	28.248	28.128	28.283	28.290	27.994	28.273	28.022	28.027	28.014	28.362	27.957
	QR	8.804	7.958	9.633	9.037	9.102	8.350	9.273	8.836	9.544	8.541	9.635	8.486	9.438	8.552	9.648	8.473
2575	FT	29.759	28.596	30.833	29.545	30.472	29.585	30.529	29.624	30.553	29.100	30.595	30.005	30.053	29.366	30.705	29.973
	FH	28.009	27.089	28.173	28.020	28.063	28.243	28.090	28.241	28.285	27.963	28.244	28.085	28.030	28.018	28.352	27.968
	QR	7.598	7.424	9.253	8.563	8.523	7.998	8.838	8.191	9.268	7.795	8.959	8.240	8.772	7.740	9.177	8.300

Table 4
Experimental data processed.

Vehicle	Distance traveled (km)	FH (mm)	FT (mm)	QR (mm)
DM061	0	28.0	32.5	10.8
	1426	28.2	31.5	9.8
	2001	28.1	30.8	9.1
	2575	28.0	30.2	8.6
DM068	0	28.0	32.5	10.8
	1050	28.0	31.8	10.0
	2253	28.0	30.2	8.5
	2576	28.0	30.0	8.4
DM082	0	28.0	32.5	10.8
	852	28.0	32.3	10.6
	1800	28.0	31.3	9.6
	2802	28.0	30.3	8.7
	3537	27.6	30.0	8.3

reference quotas (the standard values for the new unworn ORE S 1002 profile have been used). The arithmetic mean on the three vehicles MD061, MD068, MD082 has not been carried out, in order to maintain a dispersion range for the experimental data.

The experimental data, adequately processed, are summarized in Table 4. As can be seen, the flange height FH remains approximately constant because of the low mileage traveled by the vehicles, while the flange thickness FT and the flange steepness QR decrease almost linearly and highlight, according to the characteristics of the track, the wear concentration in the wheel flange.

Concerning the rail wear, the QM quota evolution is compared with a criterion present in the literature (based on the total tonnage burden on the track) [24]. Particularly a proportionality relationship between tonnage and wear holds: a rail wear of 1 mm on the rail head height every 100 Mt (millions of tons) of accumulated tonnage.

5.2. The statistical approach

The present section is an overview on the procedure used in deriving a significant statistical track description [1,10], an essential task to make possible and rationalize the approach and the simulation work on a complex railway line, as it will be showed in the following by the comparison between the two track description strategies in terms of computational effort.

In the present work the statistical approach has been exploited to draw up a virtual track of the Aosta-Pre Saint Didier line. The basic idea consists in substituting the simulation on the whole track with an equivalent set of simulations on short curved tracks (in this research activity the curved tracks length is equal to $l_{ct} = 200$ m). More precisely, the steps performed to get the statistical representation were the following:

- a set of n_{class} curve radius intervals characterized by a minimum R_{min} and a maximum R_{max} radius were identified by analyzing the database provided by RFI;
- each of these intervals was furthermore divided into n_{class} superelevation subclasses characterized by h_{min} and h_{max};
- in this case the same number n_{class} both for radius and superelevation classes is considered;
- for each radius classes a representative radius R_c was calculated as a weighted average on all the curve radii, using the length of curve as a weighting factor;
- similarly, for each superelevation subclass the corresponding representative superelevation H was chosen as a weighted average on all the curve superelevation, using the length of curve as a weighting factor;
- for each subclasses a speed value V was chosen as the minimum value between the max speed allowable in curve (equal to $V_{max} = 60$ km/h and depending on the radius, the superelevation and the vehicle characteristics) and the speed $\tilde{V}$ is calculated imposing a non-compensated acceleration of $a_{nc}^{lim} = 0.8$ m/s^2 [24,19]:

$$\frac{\tilde{V}^2}{R_c} - \frac{H}{s} g = a_{nc}^{lim} \quad V = \min(\tilde{V}, V_{max}). \tag{23}$$

  For the straight class the considered speed value, obtained from the track data, is equal to 130 km/h;
- a weighting factor p_k, calculated as explained in paragraph 4.3, was introduced for each subclass to take into account the frequency of a certain matching radius-superelevation in the track and to diversify the wear contributions of the different curves;
- the transition lengths of the real track are incorporated in the constant curvature sections next to them: in particular both the inner transition and the outer transition are divided into two equal parts and one-half is included in the previous constant curvature section while the other half is included in the succeeding one. Hence the wear is numerically evaluated on curves and straight tracks only.

As an example in Table 5 the track classification provided by the statistical approach to the Aosta-Pre Saint Didier line with $n_{class} = 7$, made up of $N_c = 30$ different classes (29 curves and the

Table 5
Data of the curvilinear tracks of the statistical analysis.

R_{min} (m)	R_{max} (m)	Superelevation $h_{min}-h_{max}$ (mm)	R_c (m)	H (mm)	V (km/h)	p_k (%)
150	175	0–19	–			
		20–39	–			
		40–59	–			
		60–79	–			
		80–99	–			
		100–119	162	110	41	0.93
		120–140	162	131	41	1.30
175	209	0–19	–			
		20–39	–			
		40–59	–			
		60–79	–			
		80–99	195	90	45	7.09
		100–119	195	103	45	7.42
		120–140	195	126	45	5.48
209	259	0–19	–			
		20–39	–			
		40–59	–			
		60–79	237	70	50	0.87
		80–99	237	83	50	8.76
		100–119	237	109	50	4.63
		120–140	237	120	50	0.47
259	342	0–19	–			
		20–39	–			
		40–59	293	50	55	0.28
		60–79	293	65	55	3.05
		80–99	293	83	55	0.90
		100–119	293	100	55	0.31
		120–140	–			
342	503	0–19	–			
		20–39	–			
		40–59	376	49	60	1.13
		60–79	376	62	60	1.26
		80–99	–			
		100–119	–			
		120–140	–			
503	948	0–19	–			
		20–39	774	24	60	1.73
		40–59	774	40	60	0.42
		60–79	–			
		80–99	–			
		100–119	–			
		120–140	–			
948	8400	0–19	3572	5	60	2.40
		20–39	3572	20	60	0.91
		40–59	–			
		60–79	–			
		80–99	–			
		100–119	–			
		120–140	–			
8400	∞	0	∞	0	130	50.65

straight track) is reported. For each one of the N_c classes of curves the unworn (i.e just re-profiled) UIC 60 rail profile canted at 1/20 has been adopted as starting condition for wear evaluation (also the wheels start from the unworn condition).

6. Results

In this section the simulation campaign carried out to study wheel and rail wear evolution will be described. Then the complete track results will be compared with the experimental data provided by Trenitalia and RFI and the comparison between the complete track results and the statistical analysis imposing a class number $n_{class}=10$ will be performed; finally a sensibility analysis of the statistical approach with respect to the n_{class} parameter will be presented.

6.1. Simulation strategy

As explained in Section 4.3, wheel and rail wear progress evolve according to different time scales and a full simulation of such events would require a too heavy computational effort. For this reason the following specific algorithm has been adopted for updating the profiles:

1. To have a good compromise between calculation times and result accuracy a suitable number of discrete steps both for wheel and for rail steps have been chosen, $n_{sw}=20$ and $n_{sr}=5$:
   (a) consequently wheel wear threshold D^w_{step} (see Section 4.3) has been fixed equal to 0.2 mm;
   (b) the value of the rail wear threshold D^r_{step} (see Section 4.3) has been set equal to 0.8 mm to obtain an appreciable rail wear during the simulations.
2. Wear evolutions on wheel and rail have been decoupled because of the different scales of magnitude:
   (a) while wheel wear evolves, the rail profile is supposed to be constant: in fact, in the considered time scale, the rail wear variation is negligible;
   (b) the time scale characteristic of the rail wear evolution, much greater than wheel wear evolution one, causes the same probability that each discrete rail profile comes in contact with each possible wheel profile. For this reason, for each rail profile, the whole wheel wear evolution (from the original profile to the final profile) has been simulated.

Based on the two previous hypotheses, the simulations have been carried out according to the following strategy:

Wheel profile evolution at first rail step : w_i^0

$$p_{1,1}\{(w_0^0\ r_0)\rightarrow(w_1^0\ r_0)\rightarrow\ldots\rightarrow(w_{n_{sw}-1}^0\ r_0)\rightarrow w_{n_{sw}}^0$$

Average on the rails $r_1^{(i+1)}$ *for the calculation of the second rail step* : r_1

$$p_{1,2}\left\{\begin{pmatrix} w_0^0 & r_0\\ w_1^0 & r_0\\ \vdots & \vdots\\ w_{n_{sw}-1}^0 & r_0\end{pmatrix}\rightarrow\begin{pmatrix} r_1^{(1)}\\ r_1^{(2)}\\ \vdots\\ r_1^{(n_{sw})}\end{pmatrix}\right\}\rightarrow r_1$$

$\vdots$

Wheel profile evolution at fourth rail step : $w_i^{n_{sr}-1}$

$$p_{5,1}\{(w_0^{n_{sr}-1}\ r_{n_{sr}-1})\rightarrow(w_1^{n_{sr}-1}\ r_{n_{sr}-1})\rightarrow\cdots\rightarrow(w_{n_{sw}-1}^{n_{sr}-1}\ r_{n_{sr}-1})\rightarrow w_{n_{sw}}^{n_{sr}-1}$$

Average on the rails $r_{n_{sr}}^{(i+1)}$ *for the calculation of the fifth rail step* : $r_{n_{sr}}$

$$p_{n_{sr},2}\left\{\begin{pmatrix} w_0^{n_{sr}-1} & r_{n_{sr}-1}\\ w_1^{n_{sr}-1} & r_{n_{sr}-1}\\ \vdots & \vdots\\ w_{n_{sw}-1}^{n_{sr}-1} & r_{n_{sr}-1}\end{pmatrix}\rightarrow\begin{pmatrix} r_{n_{sr}}^{(1)}\\ r_{n_{sr}}^{(2)}\\ \vdots\\ r_{n_{sr}}^{(n_{sw})}\end{pmatrix}\right\}\rightarrow r_{n_{sr}} \tag{24}$$

where w_i^j indicates the i-th step of the wheel profile that evolves on j-th step of the rail profile r_j (with $0\le i\le n_{sw}-1$ and $0\le j\le n_{sr}-1$). The initial profiles w_0^j are always the same for each j and correspond to the unworn wheel profile (ORE S1002).

Initially the wheel (starting from the unworn profile w_0^0) evolves on the unworn rail profile r_0 to produce the discrete wheel profiles $w_0^0, w_1^0, \ldots, w_{n_{sw}}^0$ (step $p_{1,1}$). Then the virtual rail profiles $r_1^{(i+1)}$, obtained by means of the simulations (w_i^0, r_0), are arithmetically averaged so as to get the update rail profile r_1 (step $p_{1,2}$). This procedure can be repeated n_{sr} times in order to perform all the rail discrete steps (up to the step $p_{n_{sr},2}$).

The computational effort required by the simulation strategy is the following:

(a) In wheel wear study, for each update of the rail profile r_j (n_{sr} updates), the whole wheel wear loop w_i^j (n_{sw} steps of simulation) is simulated. The computational effort results of $n_{sw} \times n_{sr} = 100$ steps both for the dynamic analysis (in Simpack Rail) and for the wear model necessary to calculate the removed material on the wheel (in Matlab).

(b) In the rail wear study the dynamic analyses are the same as that of the previous case because for each rail step the wheel profiles w_i^j are simulated on r_j in order to obtain $r_j^{(i+1)}$ and thus the updated rail profile r_{j+1} by means of an arithmetic mean. Therefore, no additional dynamical analyses are needed. In this case only the wear model steps $n_{sw} \times n_{sr} = 100$ must be simulated to get the removed material on the rail.

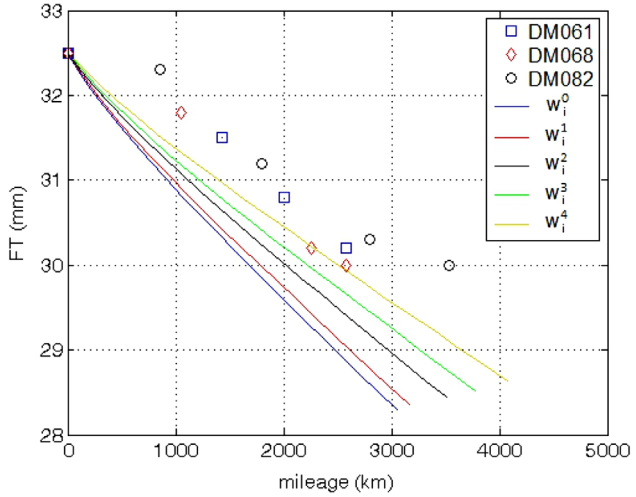

Fig. 11. Complete railway line: FT dimension progress.

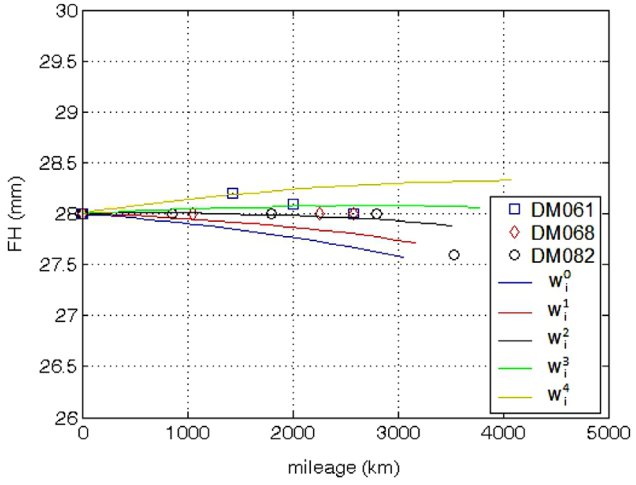

Fig. 12. Complete railway line: FH dimension progress.

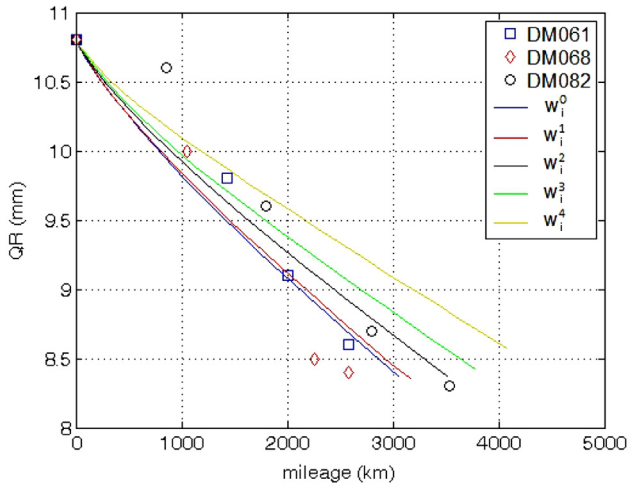

Fig. 13. Complete railway line: QR dimension progress.

6.2. Complete railway Aosta-Pre Saint Didier line results

In this paragraph the results obtained studying the whole Aosta-Pre Saint Didier line will be presented and compared with the experimental data.

6.2.1. Evolution of wear control parameters

In this section the evolution of the wheel reference quotas (flange thickness FT, flange height FH and flange steepness QR) numerically evaluated by means of the wear model will be compared with the experimental data concerning the three *DMUs*

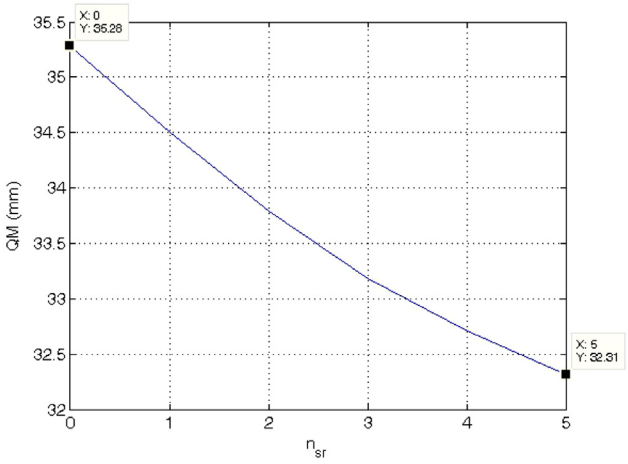

Fig. 14. Complete railway line: QM dimension progress.

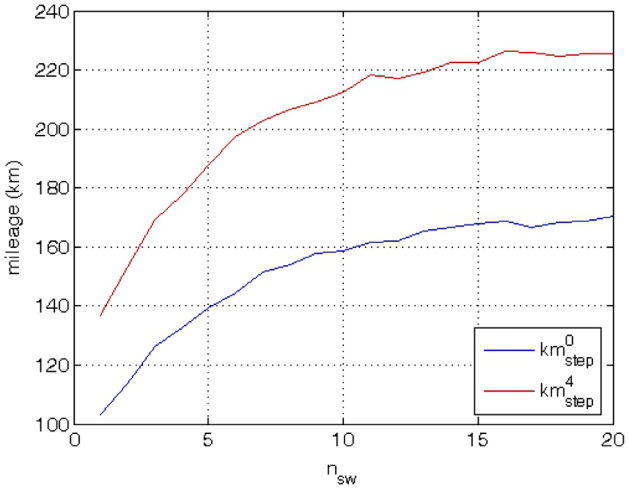

Fig. 15. Complete railway line: evolution of the km_{step}.

Aln 501 Minuetto vehicles. Furthermore, the evolution of rail reference quota QM is compared with the criterion that can be found in the literature based on the total tonnage burden on the track [24].

The progress of FT dimension, for the n_{sr} discrete steps of the rail, is shown in Fig. 11 as a function of the mileage; as it can be seen, the decrease of the dimension is almost linear with the traveled distance except in the first phases, where the profiles are still not enough conformal. The progress of the FH quota is represented in Fig. 12 and shows that, due to the high sharpness of the considered track and to the few kilometers traveled, wheel wear is mainly localized on the flange rather than on the tread; therefore the flange height remains approximately constant in agreement with experimental data. The QR trend is shown in Fig. 13: also the flange steepness decreases almost linearly except in the first phases, leading to an increase of the conicity of the flange. The evolution of the wheel control parameters remains qualitatively similar as the rail wear raises, with a slight increase of all the quotas that indicates a shift of the material removed towards the wheel tread, because of the trend of more conformal contact.

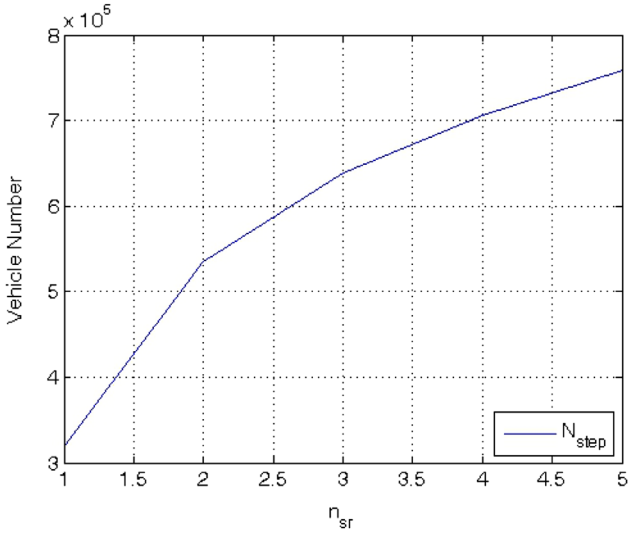

Fig. 16. Complete railway line: evolution of the N_{step}.

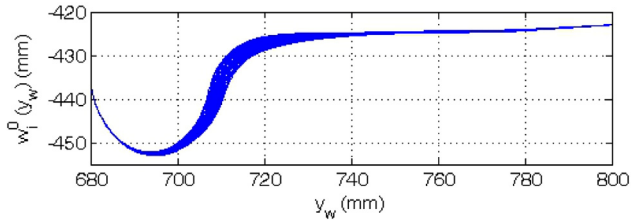

Fig. 17. Complete railway line: w_i^0 profile evolution.

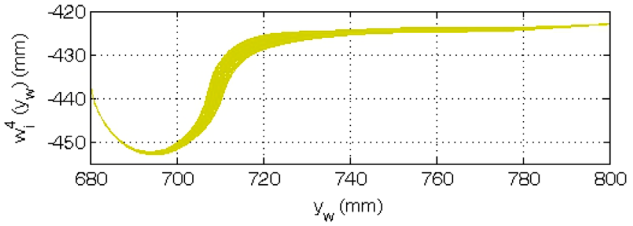

Fig. 18. Complete railway line: w_i^4 profile evolution.

The QM evolution for the analysis of rail wear is presented in Fig. 14 and shows the almost linear dependence between the rail wear and the total tonnage burden on the track. The amount of removed material on the rail head, equal to 2.97 mm, is in agreement with the criterion available in the literature (1 mm on the rail head height every 100 Mt of accumulated tonnage); the total vehicle number $N_{tot} = 2957850$ evolving on the track during the whole simulation procedure corresponds to a tonnage of $M_{tot} = N_{tot} * M_v = 310$ Mt (the vehicle mass is $M_v = 104,700$ kg (see Table 1)) (see Table 9).

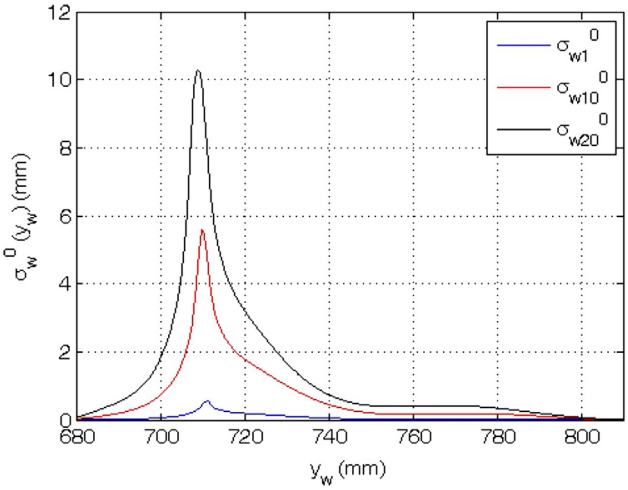

Fig. 19. Complete railway line: cumulative distributions σ_{wi}^0.

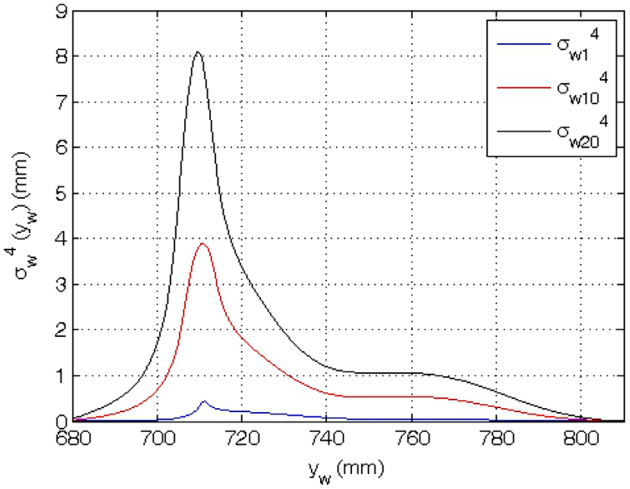

Fig. 20. Complete railway line: cumulative distributions σ_{wi}^4.

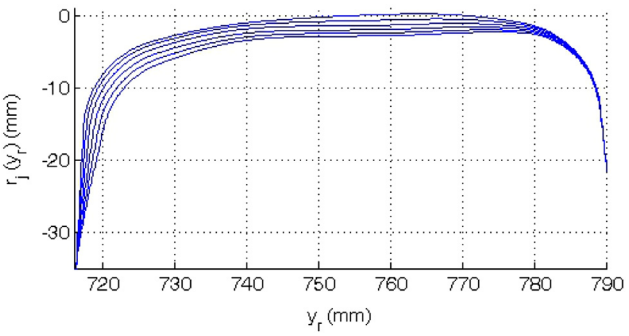

Fig. 21. Complete railway line: rail profile evolution.

In Fig. 15 the evolution of the km_{step} value as a function of the wheel discrete step number n_{sw} is illustrated (for brevity only the km_{step} related to the first and the last rail step are presented). Relating to the first rail step r_0, lower km_{step} values and their particular increasing trend in the first wheel steps indicate the higher wear rate due to the initial non-conformal contact characterizing the coupling between the new ORE S1002 wheel profile and the rail profile UIC60 with laying angle equal to 1/20; the almost constant values in the last steps (combined with higher km_{step} values) show at the same time the achievement of a more and more conformal contact as the wheel wear increases. Considering the latter rail step r_4 the same curve trend can be seen but characterized by higher km_{step} values because of the worn rail profile that leads to an initial more conformal contact than the previous case. In Fig. 16 the evolution of the N_{step} as a function of the rail discrete number n_{sr} shows that the considerations related to the variation of the contact conformity hold also for the rail wear evolution.

6.2.2. Evolution of the wheel and rail profile

Wear evolution on the wheel profiles evolving on different rail steps is presented in Figs. 17 and 18 (for reason of brevity only the profiles evolution related to the first and the last rail step are represented). As stated previously, wheel profile evolution is described by means of $n_{sw} = 20$ steps and the threshold on the removed material for each step D^w_{step} has been chosen equal to 0.2 mm. The figures show the main localization of the material removed on the wheel flange due to the quite sharp curves characterizing the Aosta-Pre Saint Didier line. Figs. 19 and 20 show the cumulative distributions of removed material in vertical direction z_w on the wheel profile at the first and the last rail step $\sigma^0_{w_{Kw}}(y_w) = \sum_{i=1}^{Kw} \sigma_i^w 0(y_w)$ and $\sigma^{n_{sr}-1}_{w_{Kw}}(y_w) = \sum_{i=1}^{Kw} \sigma_i^w n_{sr} - 1(y_w)$ as a

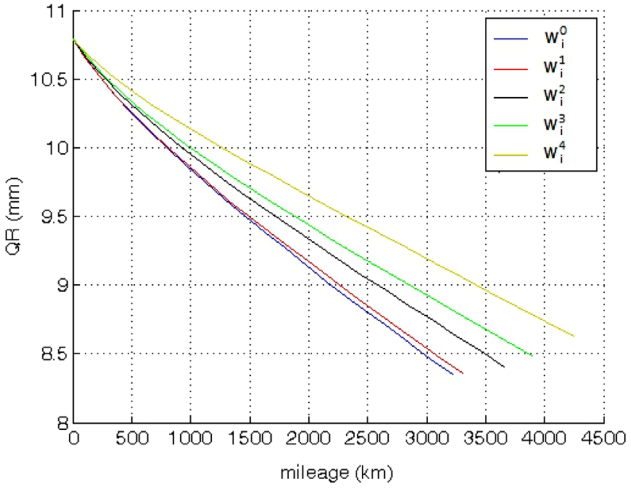

Fig. 24. Statistical analysis approach: QR dimension progress.

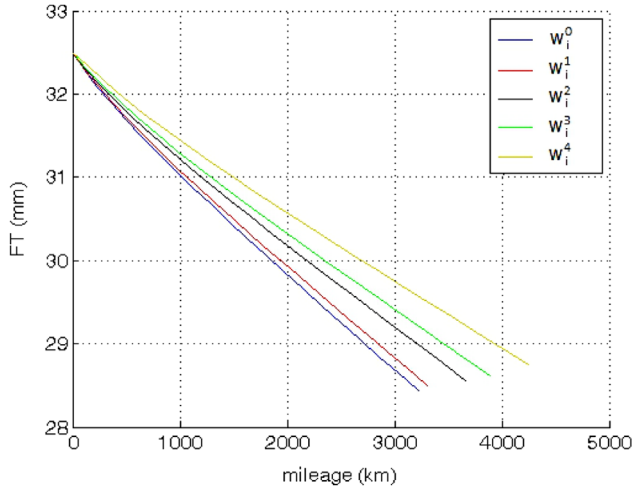

Fig. 22. Statistical analysis approach: FT dimension progress.

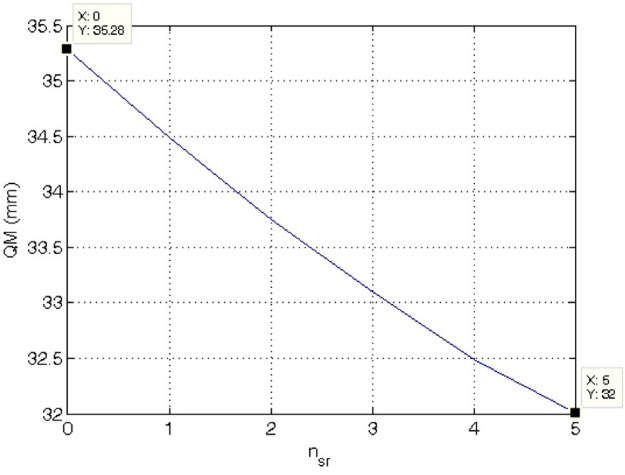

Fig. 25. Statistical analysis approach: QM dimension progress.

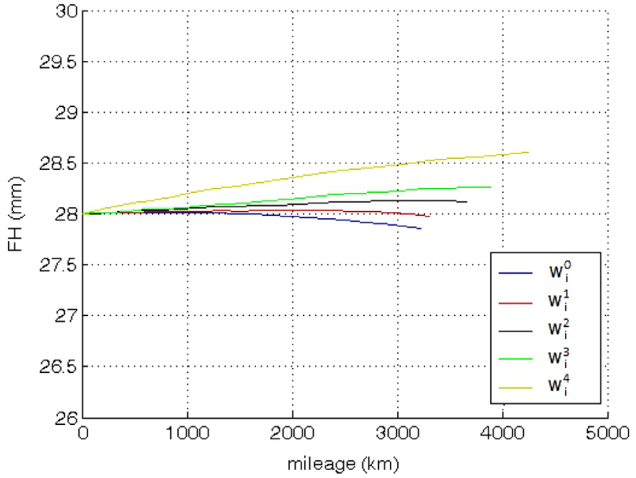

Fig. 23. Statistical analysis approach: FH dimension progress.

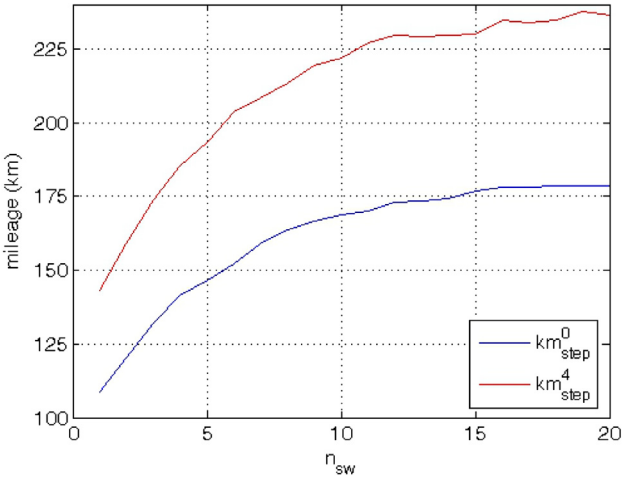

Fig. 26. Statistical analysis approach: evolution of the km_{step}.

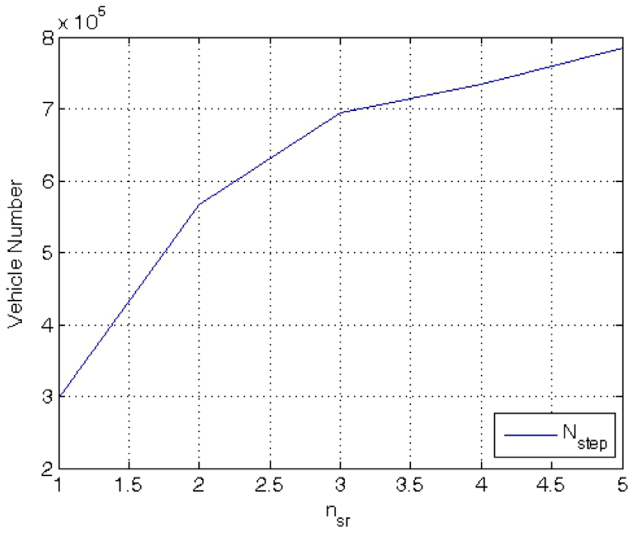

Fig. 27. Statistical analysis approach: evolution of the N_{step}.

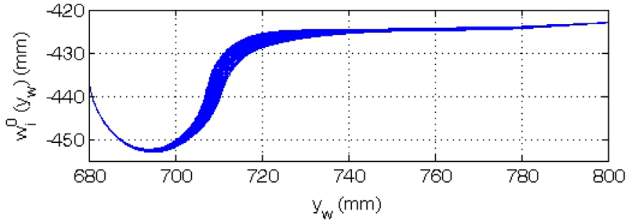

Fig. 28. Statistical analysis approach: w_i^0 profile evolution.

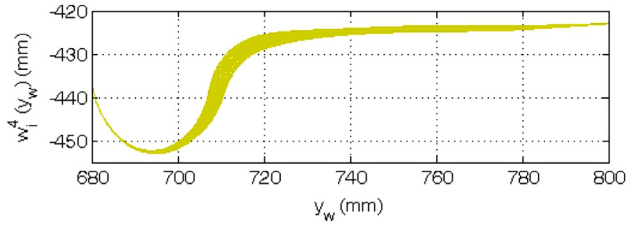

Fig. 29. Statistical analysis approach: w_i^4 profile evolution.

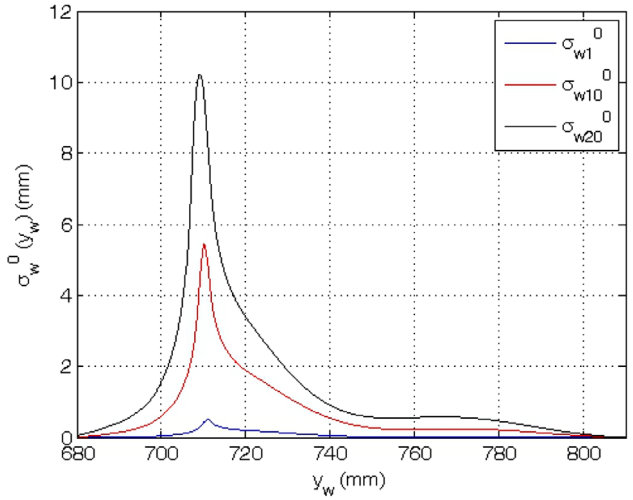

Fig. 30. Statistical analysis approach: cumulative distributions σ_{wi}^0.

function of y_w $(1 \le Kw \le n_{sw})$, where $\sigma_i^w j(y_w)$ is the removed material between two subsequent discrete steps of the wheel profile evolution (the i-th and the $(i-1)-th$ wheel discrete steps) at the j-th rail step $(0 \le j \le n_{sr}-1)$ (for reasons of brevity only the distributions characterized by $Kw = 1, 10, n_{sw}$ are represented).

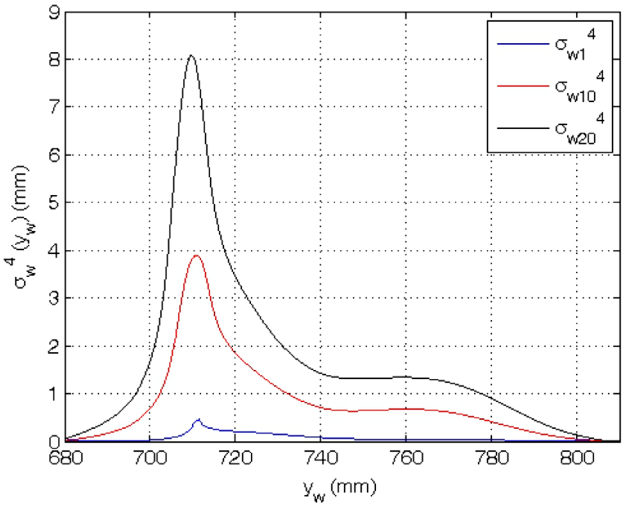

Fig. 31. Statistical analysis approach: cumulative distributions σ_{wi}^4.

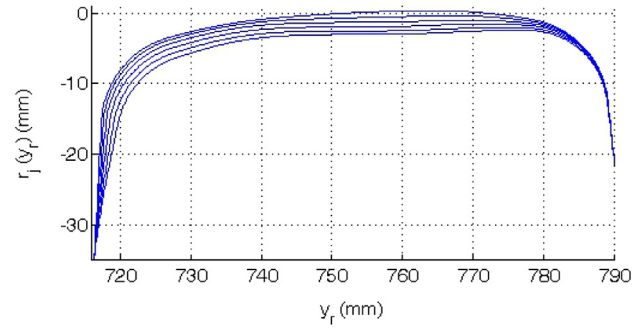

Fig. 32. Statistical analysis approach: rail profile evolution.

Table 6
Evolution of the reference quota.

Parameter	Complete railway	Statistical description $n_{class} = 10$	
	FH (mm)	FH (mm)	e (%)
km_{tot}^0	27.57	27.86	1.0
km_{tot}^1	27.73	27.98	0.9
km_{tot}^2	27.89	28.12	0.8
km_{tot}^3	28.07	28.27	0.7
km_{tot}^4	28.33	28.60	1.0
	FT (mm)	FT (mm)	e (%)
km_{tot}^0	28.30	28.43	0.5
km_{tot}^1	28.36	28.50	0.5
km_{tot}^2	28.44	28.56	0.4
km_{tot}^3	28.52	28.62	0.4
km_{tot}^4	28.63	28.75	0.4
	QR (mm)	QR (mm)	e (%)
km_{tot}^0	8.38	8.35	0.4
km_{tot}^1	8.35	8.36	0.1
km_{tot}^2	8.37	8.41	0.5
km_{tot}^3	8.43	8.48	0.6
km_{tot}^4	8.57	8.63	0.7

It can be seen that a shift of the material removed towards the wheel tread as the wheel is coupled with more and more worn rail profile due to the achievement of the conformal contact in the wheel–rail pairs.

In Fig. 21 the evolution of the rail profile is shown, described by means of $n_{sr}=5$ discrete step and with the threshold on the removed material for each step D^r_{step} equal to 0.8 mm.

6.3. Statistical analysis results

In this paragraph the results obtained with the statistical analysis approach will be presented. For this purpose a suitable value of the n_{class} parameter have to be supposed. For the Aosta-Pre Saint Didier line the value $n_{class}=10$, as will be shown in the following, represents a good compromise among track description, result accuracy and computational effort; in fact a n_{class} too high would increase the result accuracy but would increase the computational time too and would lead to a high number of curve classes quite difficult to be statistically treated.

6.3.1. Evolution of wear control parameters

Figs. 22–25 illustrate the evolution of the wear control parameters (for the n_{sr} discrete steps of the rail). The same qualitatively trend obtained with the complex railway approach both related to the conformity considerations and the localization of the worn material on the wheel flange can be seen. QM progress shows a reduction of the rail head height of 3.28 mm in agreement with the criterion presented in the literature (1 mm on the rail head height every 100 Mt of accumulated tonnage); in fact the total vehicle number $N_{tot}=3,076,200$ evolving on the curved track of the statistical description during the whole simulation corresponds to a tonnage of $M_{tot}=N_{tot}*M_v=322$ Mt (see Table 9).

The evolution of the km_{step} and N_{step} as a function of the wheel n_{sw} and rail n_{sr} step numbers can be seen respectively in Figs. 26 and 27 (for brevity only the km_{step} related to the first and the last rail step are presented) and show that the considerations related to the variation of the contact conditions due to the increase of rail wear (i.e. non conformal and conformal contact) hold also in this case.

Table 7
Evolution of the total mileage km_{tot}.

Parameter	Complete railway km_{tot} (km)	Statistical description $n_{class}=10$ km_{tot} (km)	e (%)
km_{tot}^0	3047	3219	5.6
km_{tot}^1	3163	3306	4.5
km_{tot}^2	3515	3659	4.1
km_{tot}^3	3772	3893	3.2
km_{tot}^4	4080	4244	4.0

Table 8
Evolution of the QM quota.

Complete railway QM (mm)	Statistical description $n_{class}=10$ QM (mm)	e (%)
32.31	32.00	0.6

Table 9
Total vehicle number N_{tot}.

Parameter	Complete Railway	Statistical description $n_{class}=10$	e (%)
N_{tot}	2,957,850	3,076,200	4.0

Table 10
Evolution of the wheel control parameters (quotas and km_{tot}).

Statistical description	FH (mm)	e (%)	FT (mm)	e (%)	QR (mm)	e (%)	km_{tot}(km)	e (%)
$n_{class}=4$								
km_{tot}^0	26.99	2.1	28.02	1.0	8.29	1.0	3775	23.9
km_{tot}^1	27.12	2.2	28.16	0.7	8.25	1.2	3967	25.4
km_{tot}^2	27.26	2.3	28.19	0.9	8.28	1.1	4267	21.4
km_{tot}^3	27.49	2.1	28.26	0.9	8.35	1.0	4521	19.9
km_{tot}^4	27.71	2.2	28.35	1.0	8.47	1.2	4793	17.5
$n_{class}=5$								
km_{tot}^0	27.02	2.0	28.03	1.0	8.31	0.9	3713	21.9
km_{tot}^1	27.16	2.0	28.16	0.7	8.27	0.9	3877	22.6
km_{tot}^2	27.31	2.1	28.20	0.9	8.29	1.0	4129	17.5
km_{tot}^3	27.54	1.9	28.27	0.9	8.35	0.9	4397	16.6
km_{tot}^4	27.75	2.0	28.36	0.9	8.48	1.1	4688	14.9
$n_{class}=6$								
km_{tot}^0	27.08	1.7	28.06	0.8	8.31	0.8	3620	18.8
km_{tot}^1	27.24	1.7	28.18	0.6	8.28	0.9	3743	18.5
km_{tot}^2	27.40	1.8	28.23	0.7	8.29	0.9	4038	14.9
km_{tot}^3	27.62	1.6	28.31	0.8	8.36	0.9	4237	12.3
km_{tot}^4	27.83	1.8	28.40	0.8	8.48	1.1	4569	12.0
$n_{class}=7$								
km_{tot}^0	27.11	1.7	28.09	0.7	8.31	0.8	3535	16.0
km_{tot}^1	27.26	1.7	28.19	0.6	8.29	0.8	3676	16.2
km_{tot}^2	27.43	1.7	28.25	0.7	8.30	0.9	3984	13.3
km_{tot}^3	27.65	1.5	28.33	0.6	8.36	0.8	4172	10.6
km_{tot}^4	27.85	1.7	28.42	0.7	8.48	1.0	4503	10.4
$n_{class}=8$								
km_{tot}^0	27.14	1.6	28.10	0.7	8.33	0.6	3431	12.6
km_{tot}^1	27.30	1.5	28.19	0.6	8.30	0.5	3529	11.6
km_{tot}^2	27.47	1.5	28.26	0.6	8.31	0.7	3903	11.0
km_{tot}^3	27.69	1.3	28.35	0.6	8.37	0.8	4092	8.5
km_{tot}^4	27.90	1.5	28.44	0.7	8.49	0.9	4445	8.9
$n_{class}=9$								
km_{tot}^0	27.20	1.3	28.13	0.6	8.33	0.6	3308	8.6
km_{tot}^1	27.37	1.3	28.20	0.6	8.32	0.4	3397	7.4
km_{tot}^2	27.55	1.2	28.28	0.5	8.31	0.6	3777	7.4
km_{tot}^3	27.77	1.1	28.38	0.5	8.37	0.7	4011	6.4
km_{tot}^4	27.97	1.3	28.47	0.6	8.50	0.8	4343	6.4
$n_{class}=10$								
km_{tot}^0	27.86	1.0	28.43	0.5	8.35	0.4	3219	5.6
km_{tot}^1	27.98	0.9	28.50	0.5	8.36	0.1	3306	4.5
km_{tot}^2	28.12	0.8	28.56	0.4	8.41	0.5	3659	4.1
km_{tot}^3	28.27	0.7	28.62	0.4	8.48	0.6	3893	3.2
km_{tot}^4	28.60	1.0	28.75	0.4	8.63	0.7	4244	4.0

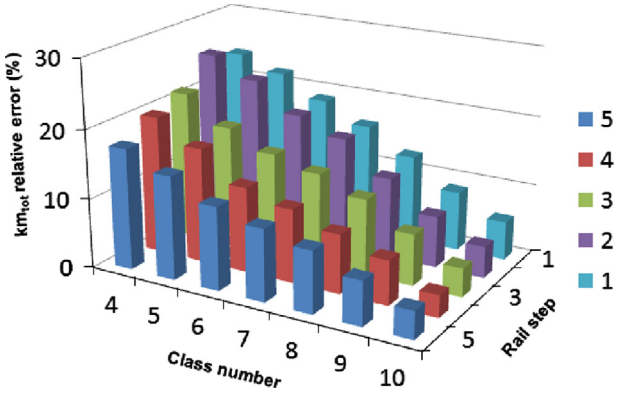

Fig. 33. Relative error of the km_{tot} parameter referred to the complete railway case.

6.3.2. Evolution of the wheel and rail profile

As can be seen in Figs. 28–31 (for reason of brevity only the profiles evolution related to the first and the last rail steps are represented) the evolution of wheel profile and the cumulative distributions of removed material are qualitatively in agreement with the complete railway approach and the same considerations of Section 6.2.2 are valid (for reasons of brevity only the figures referred to the first and the last rail steps are presented).

Table 11
Evolution of the rail control parameters (QM quota and N_{tot}).

Statistical description	QM (mm)	e (%)	N_{tot}	e (%)
$n_{class}=4$	31.58	2.3	3,797,900	28.4
$n_{class}=5$	31.63	2.1	3,641,100	23.1
$n_{class}=6$	31.69	1.9	3,543,500	19.8
$n_{class}=7$	31.75	1.7	3,398,600	14.9
$n_{class}=8$	31.83	1.5	3,309,800	11.9
$n_{class}=9$	31.86	1.4	3,188,600	7.8
$n_{class}=10$	32.00	1.0	3,076,200	4.0

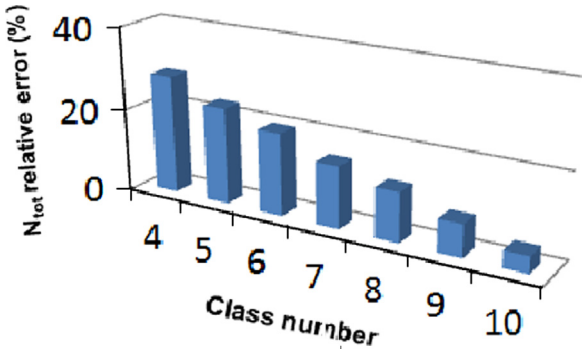

Fig. 34. Relative error of the N_{tot} parameter referred to the complete railway case.

Table 12
Processor and integrator data.

Processor	INTEL Xeon CPU X5560 2.80 GHz 24GB RAM	
Integrator	Type	ODE5
	Algorithm	Dormand-Prince
	Order	5
	Step type	fixed
	Stepsize	10^{-4} s

The evolution of rail profile obtained with the statistical approach is presented in Fig. 32.

6.4. Comparison between the complete railway line and statistical analysis

In this section a quantitative comparison among the results obtained with the complete railway line and the statistical approach with $n_{class}=10$ will be carried out. In Table 6 the final values of the wheel reference dimensions for each rail step n_{sw} are presented. The increase of the flange height as the rail profile is more and more worn, as well as the increase of the flange thickness, denotes a shift of the material removed towards the wheel tread due to the variations of the contact conditions as explained in the previous sections. The comparison of the reference dimensions shows a good consistency between the two investigated approaches with a maximum error equal to $e=1.0\%$.

Table 7 presents the evolution of the total mileage km_{tot} as a function of the rail step n_{sw} and shows a good consistency between the two considered procedures: the increase of the mileage traveled by the vehicle as the rail profile is more and more worn indicates a decrease of the wear rate due to a better conformity between wheel and rail surfaces.

In Tables 8 and 9 the comparison of the final value of the parameter QM needed to evaluate rail wear and of the total vehicle number N_{tot} is shown.

6.5. Sensibility analysis of the statistical approach

In this paragraph a sensibility analysis of the statistical approach with respect to the class number n_{class}, (the most important parameter of the track discretization) is presented. The variation range studied is $n_{class}=4-10$. Table 10 shows the final values of wear parameters and the corresponding km_{tot} values (see also Fig. 33).

Through the analysis of the data relative to the wheel presented in Table 10, for each value of n_{class} investigated, the trend of the wheel parameters shows an increase of the wheel flange dimensions according to the variation of the contact conditions explained in the previous sections (see Sections 6.2–6.4). Analogously the km_{tot} evolution trend is the same for each of the statistical analysis considered, and also the mileage increases as the rail wear increases indicating the more and more conformal contact between wheel and rail surfaces. The error e presented in Table 10 is referred to the complete railway approach (see paragraph 6.2) and shows less and less consistency between the results of the whole railway approach and the statistical analysis

Table 13
Computational time.

Railway approach	**Computational time**						
Complete track	Wheel wear evaluation			Rail wear evaluation			Total simulation time, t_T
	t_{wd}	t_{ww}	t_{wt}	t_{rd}	t_{rw}	t_{rt}	
	4 days 12 min	1 day 38 min	5 days 50 min	3 days 12 h	1 day 8 h 40 min	4 days 20 h 40 min	24 days 7 h 20 min
Statistical analysis							
$n_{class}=4$	8 min	4 min	12 min	2 h 40 min	1 h 20 min	4 h	20 h
$n_{class}=5$	11 min	4 min	15 min	3 h 40 min	1 h 20 min	5 h	1 day 1 h
$n_{class}=6$	13 min	6 min	19 min	4 h 20 min	2 h	6 h 20 min	1 day 7 h 40 min
$n_{class}=7$	15 min	7 min	22 min	5 h	2 h 20 min	7 h 20 min	1 day 12 h 40 min
$n_{class}=8$	18 min	7 min	25 min	6 h	2 h 20 min	8 h 20 min	1 day 16 h 40 min
$n_{class}=9$	21 min	9 min	30 min	7 h	3 h	10 h	2 days 2 h
$n_{class}=10$	24 min	10 min	34 min	8 h	3 h 20 min	11 h 20 min	2 days 8 h 40 min

as the n_{class} parameter decreases: in particular small n_{class} values corresponding to a rough discretization of the track lead to an important underestimation of the removed material highlighted by the increasing mileage traveled. The lower accuracy of the model and the underestimation of worn material as the track description is more and more rough are found also through the analysis of the rail control parameter QM and the number of the train evolving on the track (see Table 11 and Fig. 34) where the final values of the rail control parameter QM quota and N_{tot} are presented.

6.6. Computational effort comparison

In this section the comparison between the computational load required by the different approaches considered in this work, i.e. the complete railway line and all the analyzed statistical track descriptions ($n_{class} = 4-10$), is presented.

The characteristics of the processor and the main numerical parameters relative to the integrator used for the dynamical simulations are briefly reported in Table 12.

The mean computational times relative to each discrete step of the whole model loop are schematically summarized in Table 13 both for the complete railway line and for the statistical descriptions see also Fig. 35: the mean computational times related to the discrete steps of the whole wear model (t_{wt}, t_{rt} for wheel, see Fig. 35(a) and rail, see Fig. 35(b) respectively) are subdivided into dynamical simulation times (t_{wd}, t_{rd}) and wear simulation times (t_{ww}, t_{rw}). Obviously for all the rail computation times (t_{rt}, t_{rd}, t_{rw}) the relations $t_{rt} = n_{sw} * t_{wt}$, $t_{rd} = n_{sw} * t_{wd}$ and $t_{rw} = n_{sw} * t_{ww}$ hold and the total simulation time is $t_T = n_{sr} * t_{rt}$ where $n_{sw} = 20$ and $n_{sr} = 5$ are respectively wheel and rail discrete step numbers introduced in the previous sections.

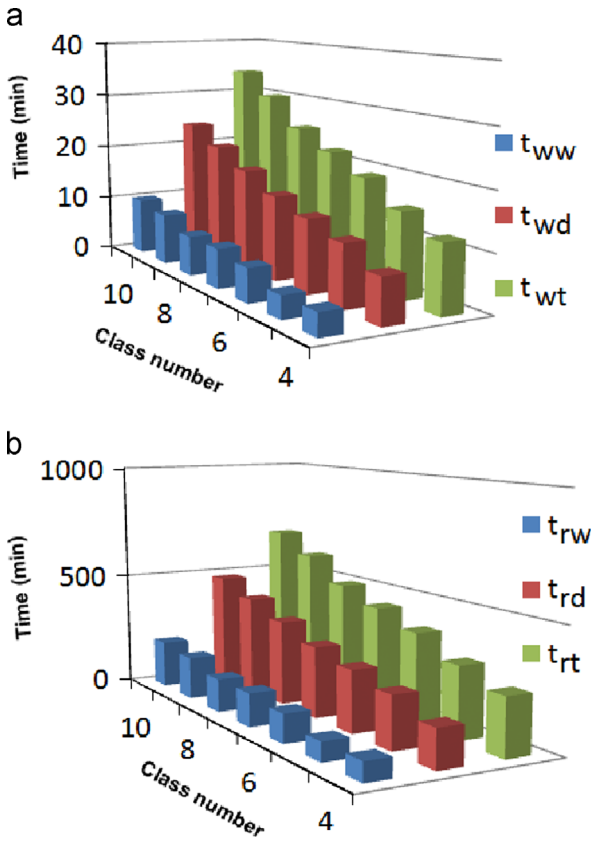

Fig. 35. Statistical analysis–computational effort comparison. (a) Wheel times. (b) Rail times.

The huge computational effort that affects the complete railway line simulation (more than 24 days for a complete simulation loop) makes this approach hardly feasible to the wear evolution studies typical of the railway field. On the contrary the statistical track description (see the Tables 10, 11 and 13) shows a high saving of computational load and at the same time a non-excessive loss of model accuracy; in particular, with a number of curve class $n_{class} = 10$, wear evaluation results are qualitatively and quantitatively in agreement with the complete line approach (a maximum error $e \simeq 5\%$ on the mileage traveled by the vehicle has been found).

In conclusion the wear model developed for the study of complex railway networks using a statistical track description approach is capable of simulating the wear evolution both on wheel and on rail surfaces with reasonable computational time and leads to a good result consistency with respect to the considered experimental data.

7. Conclusions

In this work the authors presented a complete model for the wheel and rail wear prediction in railway applications specifically developed (in the collaboration with Trenitalia S.p.A and Rete Ferroviaria Italiana (RFI), which provided the necessary technical and experimental data) for complex railway networks where the exhaustive analysis on the complete line is not feasible because of the computational load required.

The whole model is made up of two mutually interactive parts. The first one evaluates the vehicle dynamics and comprises both the multibody model of the vehicle and a global wheel–rail contact model (developed by the authors in the previous works) for the calculation of contact points and forces. The second one is the wear model which, starting from the outputs of the multibody simulations, evaluates the amount of material to be removed due to wear.

The most important aspect of the model is the track statistical approach based on the replacement of the complete railway line with a statistically equivalent set of representative curved tracks classified by radius, superelevation and traveling speed.

The whole model has been validated on a critical scenario in terms of wear in Italian railways: the ALSTOM *DMU Aln 501 Minuetto* circulating on the Aosta-Pre Saint Didier railway line. Particularly the results of the proposed model have been compared both with the complete railway network ones and with the experimental data provided by Trenitalia.

If the track discretization is accurate enough, the developed model turned out to be quite in agreement both with the experimental data and with the complete railway network model, and the evolution of all the profile characteristic dimensions described in a satisfactory way the wear progress both on wheel and on rail. As regards the track description, the statistical analysis turned out to be a good approach with a significant saving of computational time despite a very slight loss of the result accuracy if compared to the complete railway net model.

Future developments will be based on further experimental data (relative to other railway track with a higher mileage than the Aosta-Pre Saint Didier line) always provided by Trenitalia and RFI and referred to advanced wear on wheel (especially on the wheel tread) and on rail. Furthermore, measurements of the complete wheel profiles will be provided to further investigate those phenomena that cannot be highlighted only through the reference quotas.

Other analysis will be carried out in order to further validate the whole model and to better investigate the statistical approach. To this aim, further sensibility study of the statistical analysis

(mainly related to traction and braking actions, impulsive events such as the track switches and weather conditions) will be carried out. Finally, in the following phase of the research activity other wear models based on different wear laws will be studied to improve the accuracy of the whole system.

Acknowledgements

Authors would like to thank Engg. R. Cheli and G. Grande of Trenitalia S.p.A. for providing and giving the permission to edit the data relative both to the vehicle *DMU Aln 501 Minuetto* and to the wheel wear evolution; a special thanks also goes to the Engg. R. Mele and M. Finocchi of Rete Ferroviaria Italiana for the data relative to the Aosta-Pre Saint Didier line.

References

[1] SIMPACK, Official Site of Simpack Multi-Body Simulation MBS Software ⟨http://www.simpack.com/⟩, 2012.
[2] H. Krause, G. Poll, Verschleißbei gleitender und wälzender relativbewegung, Tribol. Schmier. 31 (4/5) (1984) 209–214/285–289.
[3] W. Specht, Beitrag zur rechnerischen Bestimmung des Rad- und Schienenverschleisses durch Gueterwagen Diss, RWTH Aachen, 1985.
[4] J. Pombo, J. Ambrosio, M. Pereira, R. Lewis, R.D. Joyce, C. Ariaudo, N. Kuka, A study on wear evaluation of railway wheels based on multibody dynamics and wear computation, Multibody Syst. Dyn. 24 (2010) 347–366.
[5] I. Zobory, Prediction of wheel/rail profile wear, Veh. Syst. Dyn. 28 (1997) 221–259.
[6] T. Jendel, M. Berg, Prediction of wheel profile wear, Suppl. Veh. Syst. Dyn. 37 (2002) 502–513.
[7] A. Asih, K. Ding, A. Kapoor, Modelling rail wear transition and mechanism due to frictional heating, Wear 284–285 (2012) 82–90.
[8] J. Pombo, J. Ambrosio, M. Pereira, R. Lewis, R. Dwyer-Joyce, C. Ariaudo, N. Kuka, Development of a wear prediction tool for steel railway wheels using three alternative wear functions, Wear 271 (2011) 238–245.
[9] J. Auciello, M. Ignesti, M. Malvezzi, E. Meli, A. Rindi, Development and validation of a wear model for the analysis of the wheel profile evolution in railway vehicles, Veh. Syst. Dyn. 50 (11) (2012) 1707–1734.
[10] R. Enblom, On simulation of uniform wear and profile evolution in the wheel–rail contact (Ph.D. thesis), 2006.
[11] E. Meli, S. Falomi, M. Malvezzi, A. Rindi, Determination of wheel–rail contact points with semianalytic methods, Multibody Syst. Dyn. 20 (2008) 327–358.
[12] J. Auciello, E. Meli, S. Falomi, M. Malvezzi, Dynamic simulation of railway vehicles: wheel/rail contact analysis, Veh. Syst. Dyn. 47 (2009) 867–899.
[13] H. Hertz, The contact of elastic solids, J. Reine Angew. Math. 92 (1881) 156–171.
[14] J.-F. Antoine, C. Visa, C. Sauvey, G. Abba, Approximate analytical model for hertzian elliptical contact problems, J. Tribol. 128 (2006) 660–664.
[15] J.J. Kalker, Three-dimensional Elastic Bodies in Rolling Contact, Kluwer Academic Publishers, Dordrecht, Netherlands, 1990.
[16] J.J. Kalker, A fast algorithm for the simplified theory of rolling contact, Veh. Syst. Dyn. 11 (1982) 1–13.
[17] F. Braghin, R. Lewis, R.S. Dwyer-Joyce, S. Bruni, A mathematical model to predict railway wheel profile evolution due to wear, Wear 261 (2006) 1253–1264.
[18] R. Enblom, M. Berg, Simulation of railway wheel profile development due to wear influence of disc braking and contact environment, Wear 258 (2005) 1055–1063.
[19] P. Toni, Ottimizzazione dei profili delle ruote su binario con posa 1/20, Technical Report, Trenitalia S.p.A., 2010.
[20] S. Iwnicki, The Manchester Benchmarks for Rail Vehicle Simulators, Swets and Zeitlinger, Lisse, Netherland, 1999, 2008.
[21] O. Polach, A fast wheel–rail forces calculation computer code, in: Proceedings of the 16th IAVSD Symposium, Pretoria, 1999.
[22] M. Ignesti, M. Malvezzi, L. Marini, E. Meli, A. Rindi, Development of a wear model for the prediction of wheel and rail profile evolution in railway systems, Wear 284–285 (2012) 1–17.
[23] EN 15313: Railway Applications – In-Service Wheelset Operation Requirements – In-Service and Off-Vehicle Wheelset Maintenance, 2010.
[24] C. Esveld, Modern Railway Track, Delft University of Technology, Delft, Netherland, 2001, p. 1985.
[25] O. Polach, Creep forces in simulations of traction vehicles running on adhesion limit, Wear 258 (2005) 992–1000.
[26] S. Falomi, M. Malvezzi, E. Meli, Multibody modeling of railway vehicles: innovative algorithms for the detection of wheel-rail contact points, Wear 271 (2011) 453–461.
[27] S. Magheri, M. Malvezzi, E. Meli, A. Rindi, An innovative wheel-rail contact model for multibody applications, Wear 271 (2011) 462–471.
[28] J. Auciello, M. Ignesti, L. Marini, E. Meli, A. Rindi, Development of a model for the analysis of wheel wear in railway vehicles, Meccanica 48 (3) (2013) 681–697.
[29] S. Falomi, M. Malvezzi, E. Meli, A. Rindi, Determination of wheel - rail contact points: comparison between classical and neural network based procedures, Meccanica 44 (6) (2009) 661–686.